ORIGINAL ARTICLE

Journal of Cachexia, Sarcopenia and Muscle (2021)
Published online in Wiley Online Library (wileyonlinelibrary.com) **DOI:** 10.1002/jcsm.12891

Cytoplasmic HDAC4 regulates the membrane repair mechanism in Duchenne muscular dystrophy

Alessandra Renzini[1], Nicoletta Marroncelli[1], Giorgia Cavioli[1], Silvia Di Francescantonio[1], Laura Forcina[1], Alessandro Lambridis[1], Eros Di Giorgio[2], Sergio Valente[3], Antonello Mai[3], Claudio Brancolini[2], Claudia Giampietri[4], Alessandra Magenta[5], Francesca De Santa[6], Sergio Adamo[1], Dario Coletti[1,7] & Viviana Moresi[1,8]*

[1]*Department of Anatomy, Histology, Forensic Medicine and Orthopedics, Unit of Histology and Medical Embryology, Sapienza University of Rome, Rome, Italy;* [2]*Department of Medicine, Università degli Studi di Udine, Udine, Italy;* [3]*Department of Drug Chemistry and Technologies, Sapienza University of Rome, Rome, Italy;* [4]*Department of Anatomy, Histology, Forensic Medicine and Orthopedics, Unit of Human Anatomy, Sapienza University of Rome, Rome, Italy;* [5]*Institute of Translational Pharmacology (IFT), National Research Council (CNR), Rome, Italy;* [6]*Institute of Biochemistry and Cell Biology (IBBC), National Research Council (CNR), Rome, Italy;* [7]*Biological Adaptation and Ageing, CNRS UMR 8256, Inserm U1164, Institut de Biologie Paris-Seine, Sorbonne Université, Paris, France;* [8]*Institute of Nanotechnology (Nanotec), National Research Council (CNR), c/o Sapienza University of Rome, Rome, Italy*

Abstract

Background Histone deacetylase 4 (HDAC4) is a stress-responsive factor that mediates multiple cellular responses. As a member of class IIa HDACs, HDAC4 shuttles between the nucleus and the cytoplasm; however, HDAC4 cytoplasmic functions have never been fully investigated. Duchenne muscular dystrophy (DMD) is a genetic, progressive, incurable disorder, characterized by muscle wasting, which can be treated with the unspecific inhibition of HDACs, despite this approach being only partially effective. More efficient strategies may be proposed for DMD only after the different HDAC members will be characterized.

Methods To fully understand HDAC4 functions, we generated dystrophic mice carrying a skeletal muscle-specific deletion of HDAC4 (mdx;KO mice). The progression of muscular dystrophy was characterized in mdx and age-matched mdx;KO mice by means of histological, molecular, and functional analyses. Satellite cells (SCs) from these mice were differentiated *in vitro*, to identify HDAC4 intrinsic functions influencing the myogenic potential of dystrophic SCs. Gain-of-function experiments revealed the cytoplasmic functions of HDAC4 in mdx;KO muscles.

Results Histone deacetylase 4 increased in the skeletal muscles of mdx mice (~3-fold; $P < 0.05$) and of DMD patients ($n = 3$, males, mean age 13.3 ± 1.5 years), suggesting that HDAC4 has a role in DMD. Its deletion in skeletal muscles importantly worsens the pathological features of DMD, leading to greater muscle fragility and degeneration over time. Additionally, it impairs SC survival, myogenic potential, and muscle regeneration, ultimately compromising muscle function ($P < 0.05$–0.001). The impaired membrane repair mechanism in muscles and SCs accounts for the mdx;KO phenotype. Indeed, the ectopic expression of Trim72, a major player in the membrane repair mechanism, prevents SC death (~20%; $P < 0.01$) and increases myogenic fusion (~40%; $P < 0.01$) *in vitro*; *in vivo* it significantly reduces myofibre damage (~10%; $P < 0.005$) and improves mdx;KO muscle function ($P < 0.05$). The mdx;KO phenotype is also fully rescued by restoring cytoplasmic levels of HDAC4, both *in vitro* and *in vivo*. The protective role of HDAC4 in the cytoplasm of mdx;KO muscles is, in part, independent of its deacetylase activity. HDAC4 expression correlates with Trim72 mRNA levels; furthermore, Trim72 mRNA decays more rapidly ($P < 0.01$) in mdx;KO muscle cells, compared with mdx ones.

Conclusions Histone deacetylase 4 performs crucial functions in the cytoplasm of dystrophic muscles, by mediating the muscle repair response to damage, an important role in ensuring muscle homeostasis, probably by stabilizing Trim72 mRNA. Consequently, the cytoplasmic functions of HDAC4 should be stimulated rather than inhibited in muscular dystrophy treatments, a fact to be considered in future therapeutic approaches.

Keywords Duchenne muscular dystrophy; HDAC4; HDACi; Muscle necroptosis; Membrane repair mechanism; Satellite cells

Received: 23 March 2021; Revised: 18 October 2021; Accepted: 21 November 2021
**Correspondence to: Viviana Moresi, Department of Anatomy, Histology, Forensic Medicine and Orthopedics, Unit of Histology and Medical Embryology, Sapienza University of Rome, Via Antonio Scarpa 16, 00161 Rome, Italy. Email: viviana.moresi@cnr.it*
Dario Coletti and Viviana Moresi contributed equally to this work.

Introduction

Histone deacetylase 4 (HDAC4) belongs to class IIa histone deacetylases (HDACs) within the large family of protein deacetylases, along with HDAC5, HDAC7, and HDAC9.[1] Class IIa HDACs differ in protein structure and expression patterns from the other members of the HDAC family, which include class I HDACs (HDAC1, HDAC2, HDAC3, and HDAC8), class IIb HDACs (HDAC6 and HDAC10), class IV HDACs (HDAC11), and class III HDACs (or Sirtuins), which use NAD^+ rather than Zn^{2+} as enzymatic coactivator.[1] Class IIa HDAC members, including HDAC4, do not efficiently deacetylase histones, consistently with their very low catalytic activity, due to the histidine for tyrosine substitution in their catalytic domain.[1] Class IIa HDACs function in the nucleus as transcriptional co-repressors in the NCoR/SMRT complex, driving HDAC3 onto specific class IIa HDAC target genes, or inhibiting gene transcription by blocking myocyte enhancer factor 2 activity.[1]

Differently from class I HDACs that predominantly localize in the nucleus, HDAC4 shuttles between the nucleus and the cytoplasm. HDAC4 needs to be phosphorylated at three key serine residues, in order to be exported from the nucleus and recognized by the chaperone protein 14-3-3. Another important region for HDAC4 cytoplasmic localization is its tripartite nuclear localization signal (NLS) at residues 244 to 279.[2] The nucleus-cytoplasmic translocation is usually associated with the transcriptional derepression of HDAC4 target genes. However, direct functions possibly executed by HDAC4 in the cytoplasm of skeletal muscle have been poorly described so far. Only recently, HDAC4 has been shown to deacetylate cytosolic proteins, including myosin heavy chain (MyHC) isoforms and the heat shock cognate 71 kDa protein (Hsc70),[3] thereby regulating skeletal muscle atrophy and metabolism.

Consistent with the role of stress-responsive factor, HDAC4 expression is up-regulated in skeletal muscle following denervation, because it regulates muscle atrophy and innervation by mediating several cellular responses.[4–7] HDAC4 expression is also increased in skeletal muscle following injury, where it regulates satellite cell (SC) proliferation and differentiation, as well as muscle regeneration.[8,9] Global epigenetic alterations were found in skeletal muscle of Duchenne muscular dystrophy (DMD) patients and mice, coupled to class IIa HDACs nuclear extrusion.[10] However, the specific functions of HDAC4 in muscular dystrophy are yet uncharacterized.

Duchenne muscular dystrophy is a fatal inherited muscle-wasting disease, caused by the absence of the structural protein dystrophin, as a consequence of mutations in the *DMD* gene.[11] Dystrophin, as part of the dystrophin–glycoprotein complex (DGC), anchors the extracellular matrix to the cytoskeleton. The absence of dystrophin induces progressive muscle fragility, contraction-induced damage, myofibre death, and inflammation.[11] In addition to myofibre necrosis, a recently identified form of regulated cell death, that is, necroptosis, has been reported to underpin dystrophin-deficient myofibre and SC death, as proved by the presence of high levels of the receptor interacting protein kinase-3 (Rip3).[12] As the disease progresses, myofibres are replaced by fibrotic tissue and fat infiltration, leading to muscle weakness and eventually death, usually in early adulthood.[11]

Along with dystrophin, other proteins are crucial to maintain muscle membrane integrity, including Dysferlin, MG53/Trim72 (hereafter referred to as Trim72), caveolin 3, and annexins,[13] which form a repair machinery complex that mediates sarcolemma repair in pathophysiological conditions. Indeed, if this repair process fails to compensate for structural damage, muscular dystrophy is exacerbated.[13] Consistently, enhancing the membrane repair mechanism has been proved to be beneficial in muscular dystrophies,[14] while the loss of functional Dysferlin or Trim72 makes the membrane repair mechanism less efficient, causing muscular dystrophies and myopathies *per se*.[13]

As a therapeutic strategy, a pan-HDAC inhibitor, called givinostat, is currently tested in phase III clinical trials for DMD patients, because of its beneficial effects previously demonstrated in a murine model of DMD (mdx mice). Pan-HDAC inhibitors (HDACi) have been shown to target fibro/adipogenic progenitors (FAPs) in dystrophic mice, inhibiting their adipogenic potential and favouring their ability to promote the myogenic differentiation of adjacent SCs.[15] However, pan-HDACi showed several important limitations: (i) HDACi ameliorate dystrophic conditions of young, but not adult dystrophic mice[15]; (ii) no functional improvement was reported in the phase II clinical trial study with givinostat[16]; and (iii) long-term treatment with HDACi, as required for DMD, has been associated with numerous side effects[17] that negatively affect the patients' quality of life. Some side effects or the limited effectiveness of pan-HDACi may be eliminated by identifying the specific roles of each member of the HDAC family in DMD.

In this study, we delineated the role of HDAC4 in skeletal muscle in DMD, by generating mdx mice with a muscle-specific deletion of HDAC4 (mdx;KO mice). This deletion worsened the pathological features of DMD, by increasing muscle damage and reducing muscle regeneration, ultimately leading to a decrease in muscle performance. With

DOI: 10.1002/jcsm.12891

the aim to provide a mechanistic explanation for the deleterious effect of HDAC4 deletion in dystrophic muscles, we demonstrated that cytosolic HDAC4 is responsible for the mechanism of muscle repair, SC survival, and differentiation, ultimately improving muscle regeneration and function. The HDAC4 protective role in the cytoplasm of DMD muscles is, in part, independent of its deacetylase activity and probably involves a new function influencing mRNA stability. Considering the pivotal role of HDAC4 in the cytoplasm of DMD skeletal muscle, our study provides innovative findings and suggestions for new pharmacological approaches in the treatment of dystrophic patients.

Methods

Plasmids

The following plasmids were used: pCDNA3-N2myc (Stratagene); Snap-GFP (kindly provided by Tullio Pozzan); GFP-HDAC4 (generously provided by Eric N. Olson); hHDAC4 [NM_006037.3]*L175A/Myc (CliniSciences) or GFP-hHDAC4 [NM_006037.3]*L175A (generated by Claudio Brancolini's laboratory) (named HDAC4 L/A); GFP-hHDAC4 [NM_006037.3]*L175A D840N (called GFP-HDAC4 L/A D840N) (generated by Claudio Brancolini's laboratory); pcDNA-HDAC4.3SA-FLAG (Addgene, #30486) (named HDAC4 S/A); EGFP-Dysferlin (kindly provided by Simone Spuler); and Trim72 (Myc-DDK-tagged) (named c-myc-Trim72) (OriGene).

Patients

Paravertebral or latissimus dorsi muscles from healthy subjects (two 13-year-old females and one 18-year-old male) and paravertebral muscles from 12-, 13-, and 15-year-old DMD subjects with different *DMD* mutations (exons 8–43 deletion, frameshift deletion exons 3–37, and exons 45–50 deletion, respectively) were obtained from the Myobank-AFM of the Institute of Myology (Paris, France). The 13-year-old DMD patient was under corticosteroids treatment.

Mice

Myogenin;Cre mice (kindly provided by Eric N. Olson[18]) were crossed with Hdac4$^{fl/fl}$ mice (kindly provided by Eric N. Olson), obtaining Hdac4$^{fl/fl}$ myogenin;Cre mice. The latter were crossed with the mdx (C57BL/10ScSn-DMDmdx/J) transgenic mice (Charles River Laboratories), obtaining mdx;Hdac4$^{fl/fl}$ myogenin;Cre mice and mdx;Hdac4$^{fl/fl}$ mice (referred to as mdx;KO and mdx mice, respectively). In all the experiments, female mdx;KO and mdx littermates were compared. In addition, aged-matched, female Hdac4$^{fl/fl}$ mice (referred to as CTR mice) were used as control healthy mice. Mice were treated in strict accordance with the guidelines of the Institutional Animal Care and Use Committee, as well as national and European legislation, throughout the experiments. Animal procedures followed the 3Rs principles in alignment with the Directive 2010/63/EU of the European Union, and the protocols used were approved by the Italian Ministry of Health (authorization # 853/2016-PR).

Functional analyses

The treadmill test was performed by using the Exer-6M (Columbus Instruments) with a downhill exercise protocol to exhaustion, as previously described.[19] For 16-month-old mice, the protocol was adapted as previously reported.[20] n = 6 mice per condition at each time point were analysed.

DNA delivery by electroporation

The electroporation was performed in 5.5-month-old mice, to allow sufficient time for the expression of the ectopic genes and for the recovery from electroporation, in order to analyse the muscles at 6 months of age. In anaesthetised mice, gastrocnemius (GA) muscles were exposed, injected with 12 μg of DNA in 5% mannitol solution directly in two-thirds of the muscle, and immediately subjected to electric stimulation using a pulse generator (ECM 830, BTX), equipped with 3 × 5 mm of genepaddle electrodes, placed at opposite sides of the muscle. Electroporation was performed by delivering six electric pulses of 10 V each, with a fixed duration of 20 ms and an interval of 200 ms between the pulses. At least n = 4 mice per condition were used.

Serum CK assay

Serum samples were collected from blood drawn via cardiac puncture from 6-week-old mice and stored at −80°C until used. Serum was assayed using a colorimetric Creatine Kinase Activity Assay Kit, according to the manufacturer's protocol (RayBiotech). n = 7 mice per condition were used.

Sarcolemma membrane integrity by Evan's blue dye uptake

Mice were intraperitoneally injected with 10 μL/g body weight of a 1% Evan's blue dye (EBD) solution in phosphate-buffered saline (PBS) (Sigma-Aldrich) 8 h before the sacrifice. EBD signal was recorded on formalin-fixed cryosections by using a 516/560 excitation/emission pair by fluorescence microscopy. n = 3–5 mice per condition were analysed.

DOI: 10.1002/jcsm.12891

Histological analyses

Gastrocnemius muscles were dissected, embedded in tissue freezing medium (Leica), and frozen in isopentane pre-cooled with liquid nitrogen. Serial sections (9 μm) of the mid-belly of GA muscles were obtained by using a Leica cryostat. *n* = 3–5 mice per condition were analysed. Haematoxylin and eosin (H&E) staining (Sigma-Aldrich) was performed according to the manufacturer's instructions.

Immunofluorescence

Cryosections or single myofibres were fixed in formalin buffered solution 10% (Sigma-Aldrich) for 10 min at room temperature (RT), then washed and blocked with 1% bovine serum albumin (BSA) (Sigma-Aldrich) for 30 min or with 10% goat serum for 30 min. Samples were then incubated overnight at 4°C with one of the following antibodies, diluted in 1% BSA: 1:50 rabbit polyclonal anti-laminin antibody (clone LAM-89, Sigma-Aldrich), 1:400 rabbit anti-GFP (Polyclonal, Thermofisher), 1:50 c-Myc antibody (clone 9E10, Santa Cruz), 1:40 anti-Myh3 antibody (clone BF45, Hybridoma Bank), 1:100 anti-Dysferlin antibody (clone JAI-1-49-3, Abcam), 1:80 anti-Trim72 antibody [Polyclonal, Synthetic peptide corresponding to Human MG53 aa 288–337 (internal sequence), Abcam], and 1:10 sarcomeric MHC antibody (clone MF 20, Developmental Studies Hybridoma Bank). To detect the primary antibodies, incubation with a 1:500 dilution of anti-rabbit-Alexa 488 or Alexa555 (Thermo Fisher Scientific) secondary antibody in 1% BSA for 1 h at RT or with 1:1000 biotin-conjugated secondary antibody (Jackson ImmunoResearch) for 45 min at RT, followed by 1:2500 streptavidin antibody (Jackson ImmunoResearch) for 30 min at RT was performed. For IgG staining, after blocking, muscles were incubated with a 1:500 dilution in 1% BSA of anti-mouse-Alexa 555 (Thermo Fisher Scientific) secondary antibody, for 1 h at RT. An additional step of permeabilization was used for c-Myc (1% BSA/0.2% Triton/PBS for 30 min), and alternative fixation with cold acetone for 5′ at −20°C for Myh3, or cold methanol for 5′ at −20°C for Dysferlin and Trim72 were used; 0.5 μg/mL Hoechst 33 342 (Sigma-Aldrich) or DAPI were used to stain nuclei. For single myofibres, an additional step was added to minimize formalin background by using 1% glycine in PBS. Coverslips were mounted with 60% glycerol in Tris HCl 0.2 M pH 9.3. Photographs were acquired using an Axio imager A2 system equipped with an Axiocam HRc, with Axiovision Release 4.8.2 software (Zeiss). At least *n* = 3 biological samples per genotype were analysed. For neuromuscular junction (NMJ) evaluation, freshly isolated GA muscles were fixed in 10% neutral buffered formalin solution (Sigma-Aldrich), overnight at 4°C. Small bundles of myofibres were isolated under the dissecting microscope as previously described.[21] The pre-synaptic terminal was labelled with mouse anti-neurofilament (1:200; SMI-312; BioLegend) and rabbit anti-synaptophysin (1:200; Thermo Fisher Scientific). TRITC AP donkey anti-mouse IgG (1:200; Jackson ImmunoResearch Laboratories, Inc.) and Cy5 AP donkey anti-rabbit IgG (1:400; Jackson ImmunoResearch Laboratories, Inc.) secondary antibodies were used to visualize neurofilaments and synaptic vesicles, respectively. AChRs were labelled with Alexa Fluor 488-conjugated α-bungarotoxin (10 nM; Molecular Probes). Z-stack images were obtained at sequential focal planes 3 μm apart using a confocal microscope (Laser Scanning TCS SP2; Leica). NMJ morphology was assessed in terms of total bungarotoxin stained area, total synaptophysin stained area, endplate area, and NMJ occupancy index (synaptophysin/bungarotoxin area * 100).[22]

For each genotype, a minimum of 40 endplates were evaluated from randomly selected microscopic fields. Representative images shown in the figures are flattened projections of Z-stack images.

Morphometric analyses

Photographs were acquired using an Axio imager A2 system equipped with an Axiocam HRc, with Axiovision Release 4.8.2 software (Zeiss), at standard 1300 × 1030 pixel resolution. The myofibre cross-sectional area (CSA) was quantified on stained sections from the mid-belly of GA or diaphragm muscles by using ImageJ software. *n* = 3–6 mice per condition were used. The entire muscle section was quantified for each replicate. Ten fields per sample were analysed for the *in vitro* analyses. Muscle cell terminal differentiation was quantified by differentiation index, that is, the number of myonuclei in MHC+ cells, over total nuclei, and fusion index, that is, the number of myonuclei within myotubes, over total nuclei. A myotube was defined as having ≥2 nuclei in the same cytoplasm. Ten fields for at least three different replicate samples were analysed.

Satellite cell isolation and culture conditions

Satellite cells were isolated from 3-week-old mice by using MACS microbeads technology (GentleMACS, Miltenyi Biotec), according to the manufacturer's protocol. Briefly, skeletal muscle was cut into small pieces and put in a C-tube with the enzyme cocktail of the dissociation kit (# 130-098-305). Muscles were then subjected to mechanical disaggregation in the GentleMACS dissociator, at 37°C. Following dissociation, samples were filtered to remove contaminant undigested muscle fragments from the single-cell suspension. SCs were then isolated using the Satellite Cell Isolation Kit (#130-104-268), by depletion of non-target cells, which were magnetically labelled with a cocktail of monoclonal

DOI: 10.1002/jcsm.12891

antibodies conjugated with MACS MicroBeads. SCs were plated on 0.01% collagen (Sigma-Aldrich)-coated dishes or on Matrigel (Corning)-coated glasses in Dulbecco's modified Eagle's medium (DMEM) supplemented with 20% horse serum (Sigma-Aldrich),100 U/mL penicillin (Sigma-Aldrich), 100 μg/mL streptomycin (Sigma-Aldrich), and 3% of chicken embryo extract as a growing medium (GM).[8] After 48 h, the medium was replaced with a differentiation medium (DM) (GM diluted 1:10). SCs derived from at least three mice per condition were used in *in vitro* experiments.

Single myofibre isolation and culture conditions

Single myofibres were isolated from the EDL muscles of 6-week-old mice as previously described.[23] Briefly, EDL muscles were dissected and incubated in DMEM (Sigma) containing 0.2% collagenase I (Sigma) for 45 min at 37°C. Myofibres were detached using gentle trituration with a glass pipette and washed several times with DMEM with 100 U/mL penicillin (Sigma-Aldrich) and 100 μg/mL streptomycin (Sigma-Aldrich). Single myofibres derived from n = 2 mice per each condition were used.

DNA delivery by transfection

For transient transfection, 3×10^5 mdx;KO SCs were seeded in 35-mm-diameter plates. After 1 h, cells were transfected with 4 μg of total DNA, using Lipofectamine (Invitrogen), following the manufacturer's instructions, except for the replacement of the medium 6 h after transfection. When needed, Snap-GFP plasmid was combined with the plasmid of interest in a 1:3 ratio, to monitor the transfection efficiency. Transfected cells were cultured in GM for 48 h and then shifted to DM. Preliminary experiments demonstrated that the overexpression of pCDNA3-N2myc plasmid did not affect mdx;KO cell differentiation and that pCDNA3-N2myc or GFP as empty vectors could be used interchangeably. SCs isolated from n = 4 mice per each transfection experiment were used. From each mouse, SCs were splitted in two groups and transfected either with the plasmid of interest or with control plasmid.

mRNA stability assay

Terminally differentiated mdx and mdx;KO myotubes were treated with 2.5 μM Actinomycin D (ActD) (Sigma-Aldrich) and then harvested 20, 40, 60, and 180 min later. Total RNA was extracted and analysed by real-time PCR; 18S was used as the housekeeping gene in these experiments. SCs isolated from three mice per condition were used.

Tunel assay

Tunel assay was performed using the ApopTag® Fluorescein In Situ Apoptosis Detection Kit (Merck Millipore) following the manufacturer's instructions. n = 4 mice per condition were used.

RNA extraction and real-time PCR

Total RNA was isolated and purified from 30 to 50 mg of GA muscles or cells by using Trizol (Invitrogen), following the manufacturer's protocol. One microgram of total RNA was retrotranscribed to cDNA by using the PrimeScript™ RT Reagent Kit (Takara). Real-time PCR was performed with the SDS-ABI Prism 7500 (Applied Biosystems) by using the TB Green™ Premix Ex Taq™ mastermix (Takara) and the following primers.

Hdac4: GTCTTGGGAATGTACGACGC; GTTGCCAGAGCTGCTA TTTG; Dysferlin: GAATCCCCTGTTCTCCTCGC; CAAAGCCCTCAT TGGACACG; Trim72: GCCTCAAGACACAGCTTCCA; TGCTTCA CGGTCCAGAGAAC; 18S: GCAATTATTCCCCATGAACG; GGGA CTTAATCAACGCAAGC; Gapdh: ACCCAGAAGACTGTGGATGG; CACATTGGGGGTAGGAACA; Myh3: TCGTCTCGCTTTGGCAA; TGGTCGTAATCAGCAGCA; MCK: CACCATGCCGTTCGGCAA CA; GGTTGTCCACCCCAGTCT; c-myc: TACCAGGCTGCGCGCAA; AGCGAGTCCGAGGAAGGA; AChRγ: GGAGAAGCTAGAGAA TGGTCC; CCCACTGACAAAGTGACT CTGC; Musk: GTCCCTCCT CCGTGGTTTTC; CAGGACTGCATCACACACCT; MEF2C: GCACC AACAAGCTGTTCCAG; CAGATCTCCGCCCATCAGAC; Dach2: ACTGAAAGTGGCTTTGGATAA; TTCAGACGCTTTTGCATTGTA; p21: AGCGCGTTCGGAGCCTA; CCGTTTTCGGCCCTGAGA; Sharp1: AATTGACAACACTGGGGCATT; GGAGGCGAGAA AGAAAAACCG; Myh7: AGTCCCAGGTCAACAAGCTG; TTC CAC CTA AAG GGC TGT TG; Myh2: AGT CCC AGG TCA ACA AGC TG; GCA TGA CCA AAG GTT TCA CA; Myh4: AGT CCC AGG TCA ACA AGC TG;TTT CTC CTG TCA CCT CTC AAC A; HDAC5: GAAGCACCTCAAGCAGCAGCAGG; CACTCTCTTTGCTCTTCTCC TTGTT; HDAC7: AGCTGGCTGAAGTGATCC; TCACCATCAGCCT CTGAG; HDAC9: TCAGAGGTTCCTATGGGCCTG; TGGAGACGT TCCACTGAGGG; NCAM: GAGCGCTCTGTACTTGACCA; AGAGG ACGGGAACTCCATCA.

RNA 18S or Gapdh were used as loading control. At least n = 4 mice per each condition were used.

Protein extraction and western blot analyses

Muscles were dissected, minced, and homogenized in lysis buffer (50 mM Tris–HCl pH 7.4, 1 mM EDTA, 150 mM NaCl, 1% Triton) supplemented with protease and phosphatase inhibitors. For protein subcellular fractionation, the protocol described in literature[24] was used. Briefly, muscles were homogenized in STM buffer (250 mM sucrose, 50 mM Tris–-

DOI: 10.1002/jcsm.12891

HCl pH 7.4, 5 mM $MgCl_2$) supplemented with protease and phosphatase inhibitors. This homogenate was maintained on ice for 30 min, vortexed at maximum speed for 15 s, and then subjected to serial centrifugations as follows: the homogenate was centrifuged at 800 *g* for 15 min; the resulting supernatant was centrifuged at 800 *g* for 10 min; the resulting pellet was combined with the first pellet to isolate the nuclear fraction (NF), while the resulting supernatant was processed as follows to yield the cytosolic fraction: centrifugation at 11 000 *g* for 10 min; the resulting supernatant precipitated in 100% acetone at −20°C for 2 h, followed by centrifugation at 12 000 *g* for 5 min; the resulting pellet was then resuspended in STM buffer. The NF was extracted as follows: the pellet of the NF was resuspended in STM buffer, vortexed at maximum speed for 15 s, and washed twice at 500 *g* for 15 min and at 1000 *g* for 15 min. The latter pellet was resuspended in NET buffer (20 mM HEPES pH 7.9, 1.5 mM $MgCl_2$, 0.5 M NaCl, 0.2 mM EDTA, 20% glycerol, 0.5% Triton-X-100) supplemented with protease and phosphatase inhibitors, vortexed, and incubated on ice for 1.5 h. Lastly, the NF was sonicated on ice for 3 × 5 s, and the lysate was centrifuged at 9000 *g* for 30 min. The resulting supernatant was the final NF extract. All procedures were carried out at 4°C. The cytosolic and NFs were aliquoted and frozen at −80°C until analysed.

Protein concentration was quantified using a BCA Protein Assay Kit (Thermo Fisher Scientific). For each sample, 40–70 μg of proteins were run on nUView Tris-Glycine gels. The gels were transferred to nitrocellulose membranes and protein bands were visualized under UV light. The whole signal of the entire lane has been used for loading and transfer control. Membranes were blocked with 5% BSA in TBST and blotted with different primary antibodies. After washing in TBST, membranes were incubated with HRP-conjugated secondary antibodies (BIO-RAD), and signals were detected by using ECL chemistry (Cyanagen). Images were acquired on a ChemiDoc MP imaging system (BIO-RAD) with Image Lab 5.2.1 software. The following primary antibodies were used: HDAC4 (clone H-92, Santa Cruz), Gapdh (clone 6C5, Santa Cruz), Dysferlin (clone JAI-1-49-3, Abcam), Trim72 [Polyclonal, Synthetic peptide corresponding to Human MG53 aa 288–337 (internal sequence), Abcam], Rip3 [Polyclonal, Synthetic peptide corresponding to Mouse RIP3 (C terminal), Abcam], Myh3 (clone F1.652, Developmental Studies Hybridoma Bank), Myogenin (clone F5D-s, Developmental Studies Hybridoma Bank), and H3 (Synthetic peptide corresponding to the carboxy-terminal sequence of human histone H3, Cell Signaling). *n* = 3–5 mice per condition were used.

Co-immunoprecipitation

Co-immunoprecipitation (Co-IP) was performed on cytoplasmic cell extracts from c-myc-Trim72 transfected mdx myotubes by standard, non-denaturing, procedures. In brief, cells, were lysed in cytoplasmic lysis buffer (50 mM Tris pH 8; 150 mM NaCl; 0.1 mM EDTA pH 8) supplemented with protease and phosphatase inhibitors for 15 min; NP-40 was added, and cells were centrifugated to pellet nuclei. Cytosolic supernatant was sonicated using a manual sonicator UP100 (1 pulse/20 s/40% amplitude) and centrifuged at 16 000 *g* for 10 min. Protein concentration was quantified using a BCA Protein Assay Kit (Thermo Fisher Scientific). Cell extracts were precleared with Dynabeads™ protein G (Thermofisher) for 45 min at 4°C, immunoprecipitated with 2 μg of anti-c-myc or 2 μg of normal mouse IgG (Santa Cruz) for 2 h at 4°C, and incubated with protein G. Immunoprecipitates were extensively washed with IP lysis buffer (50 mM Tris pH 8; 150 mM NaCl; 1 mM EDTA pH 8; 1 mM EGTA) supplemented with protease and phosphatase inhibitors and resuspended in Laemmli sample buffer. SCs derived from *n* = 2 mice were used.

Histone deacetylase activity assay

Histone deacetylase activity was evaluated by using different fluorogenic substrates specific for class I, class IIa, or class I/IIb HDACs. These specific substrates were synthesized according to the literature and the assays were performed as previously described.[25] Briefly, GA muscles were dissected, minced, and homogenized in PBS (pH 7.4) containing 0.5% Triton X-100, 300 mM NaCl, and protease/phosphatase inhibitor cocktail (Thermo Fisher Scientific), incubated on ice 45 min, and sonicated prior to clarification by centrifugation. Protein concentration was determined using a BCA Protein Assay Kit (Thermo Fisher Scientific). Extracts were diluted into PBS buffer in 100 μL total volumes in 96-well plate (30 μg protein per well). Where indicated, TSA (1 μL of 100× DMSO stock solution) or corresponding volumes of DMSO were added, followed by 45 min incubation at 37°C. Substrates were added (5 μL of 1 mM DMSO stock solution), and the plates were returned to the 37°C incubator for 3 h. Then, 50 μL per well of developer/stop solution were added (PBS with 1.5% Triton X-100, 3 μM TSA, and 0.75 mg/mL trypsin), allowing an additional 20 min incubation at 37°C. To detect fluorescent signal, the Glowmax (Promega) instrument was used, with excitation and emission filters of 360 and 460 nm, respectively. Background signals from buffer blanks were subtracted, and data were normalized as needed using appropriate controls. *n* = 6 mice per condition were used.

Statistics and program

Statistical significance was determined by using two-tailed Student's *t*-test when two conditions needed to be compared, or with one-way analysis of variance (ANOVA), followed by

DOI: 10.1002/jcsm.12891

Tukey's HSD test as a post hoc test, when more than two conditions needed to be compared. All values were expressed as mean ± standard error of the mean (SEM). VassarStats, a statistical computation website (http://vassarstats.net/), was used for the statistical analyses. All the graphs were created by using GraphPad Prism 6 program. *Figure* 8 was created with BioRender (https://biorender.com/).

Differences between mdx and mdx;KO mice were confirmed in independent experiments, that is, the analyses were carried out using independent litters; in addition, *n* represents an independent biological sample (a distinct mouse) and is not a mere technical replicate.

Results

Histone deacetylase 4 expression and activity is modulated in skeletal muscle of mdx mice

To investigate the role of HDAC4 in DMD, mice carrying the skeletal muscle-specific deletion of HDAC4 ($Hdac4^{fl/fl}$; myogenin-Cre, hereafter referred to as HDAC4mKO) were crossed with mdx mice, obtaining mdx;KO mice. Worth noting, HDAC4mKO do not have any obvious phenotype.[7] Western blotting (WB) analysis revealed an increase in HDAC4 expression in the GA muscles of mdx mice, as compared with healthy controls (CTR), and a significant decrease of HDAC4 in mdx;KO muscles, as compared with mdx mice at 6 weeks of age (*Figure* 1A and Supporting Information, *Figure* S1A), or in mdx;KO primary myotubes *in vitro* as compared with mdx myotubes (*Figures* 1B and S1B). To study the subcellular localization of HDAC4 in adult mdx muscle, a WB for the nuclear and cytoplasmic fractions was performed. HDAC4 mostly localized in the cytoplasm (*Figures* 1C and S1C), as also confirmed by immunofluorescence (IF) on primary mdx myotubes (*Figure* 1D). Consistently, the transcription of HDAC4 target genes, that is, MEF2C, Dach2, p21, and Sharp1, did not result altered when comparing mdx and mdx;KO mice (*Figure* S1E). Importantly, HDAC4 expression also resulted up-regulated in skeletal muscles of DMD patients (*Figures* 1E and S1D).

To exclude any compensatory effects of other HDAC members in the mdx;KO mice, the catalytic activities of different HDAC families were quantified in muscle lysates, by using specific fluorogenic substrates containing acetyl-lysine groups.[25] To verify the specificity of the reactions, we added HDACi trichostatin A (TSA), which blunted the class I and class IIb activities, but not that of the class IIa, as previously reported.[25] The activities of several HDAC classes resulted up-regulated in mdx muscles if compared with CTR; HDAC4 deletion in skeletal muscle resulted in a significant reduction in class IIa activity, as expected, but did not affect class I and IIb HDAC activities (*Figure* 1F). Of note, among class IIa members, only *Hdac4* expression was significantly modulated among CTR, mdx, and mdx;KO muscles (*Figure* 1G), pointing to a specific role for HDAC4 in muscular dystrophy.

Histone deacetylase 4 deletion in skeletal muscle worsens muscular dystrophy in mdx mice

To determine if the deletion of HDAC4 affects the onset and/or the progression of muscular dystrophy, mdx;KO and age-matched mdx mice were analysed over time. The kinetics of the EBD-positive area in mdx;KO muscles showed a significantly higher muscle damage at all the time points analysed, with the exception of the 6 month time point (*Figure* S2A). Based on the well-known peaks of muscle damage occurring in mdx mice at 3 and 6 weeks, muscle damage was further analysed at these time points in mdx;KO mice by IgG staining (*Figure* 2A), as well as by quantifying the serum creatine kinase release in the serum at 6 weeks (*Figure* 2B). The muscle degeneration we observed was probably due to muscle necroptosis, as proved by increased levels of Rip3 in muscle extracts of mdx;KO mice as compared with mdx littermates (*Figures* 2C and S2B).

Muscle regeneration was evaluated by quantifying the area occupied by regenerating myofibre with central nuclei in cross-sectioned GA muscles. Mdx;KO muscles showed a decrease of the regenerating area at all the time points analysed, with significant differences at 6 weeks and 16 months as compared with mdx littermates (*Figure* S2C). Such compromised muscle regeneration was confirmed by reduced myogenin protein levels, as observed by WB analyses in mdx;KO muscles compared with mdx littermates (*Figures* 2D and S2D), and further proved by a reduced embryonic myosin heavy chain (Myh3)-positive area observed by IF, at 6 weeks (*Figure* 2E). All of the above was confirmed by the similar results obtained in the diaphragm muscle (*Figure* S3).

Given the clinical relevance of muscle function loss, which ultimately is responsible of the death of dystrophic patients, we also verified whether the observed histological and molecular differences between the two genotypes resulted in differences in muscle performance. The latter was evaluated at 6 weeks, as well as 6 and 16 months of age, by subjecting mice to a downhill treadmill exercise protocol while measuring the running time and the distance to exhaustion. Importantly, mdx;KO mice performed worse at all the time points for both parameters compared with mdx littermates (*Figure* 2F). Overall, these results indicated a global and severe loss of muscle performance in the absence of HDAC4.

Histone deacetylase 4 affects skeletal muscle cell survival and myogenic potential in mdx mice

Based on the observed decrease in skeletal muscle regeneration in mdx;KO mice, we wondered whether HDAC4 af-

DOI: 10.1002/jcsm.12891

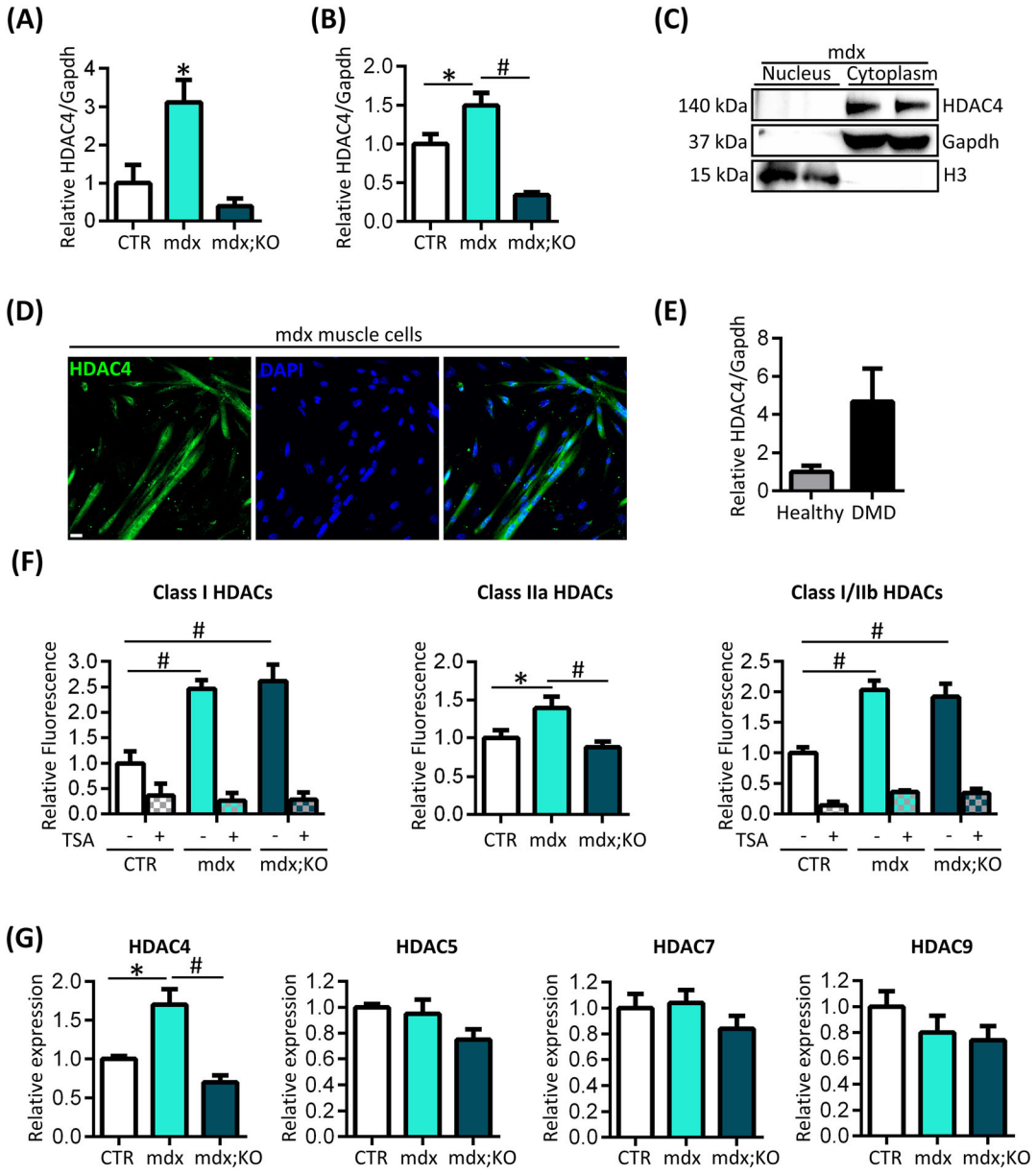

Figure 1 HDAC4 expression and activity is modulated in the skeletal muscle of mdx and mdx;KO mice. (*A*) Densitometric analysis of the WB bands for HDAC4, over Gapdh, in 6-week-old healthy controls (CTR), mdx, or mdx;KO GA muscles. Gapdh was used as loading control. The residual expression of HDAC4 in mdx;KO muscles is due to the presence of tissues other than muscle in the protein extract. Data are expressed as mean ± SEM, over CTR mice. n = 3 mice per condition. One-way ANOVA reveals a significant effect and interaction: $^{*}P < 0.05$ mdx versus CTR and mdx;KO by Tukey's HSD test. (*B*) Densitometric analysis of the WB bands for HDAC4, over Gapdh, in CTR, mdx, and mdx;KO primary myotubes. Data are presented as mean ± SEM, over mdx cells. n = 3 mice for each genotype. One-way ANOVA reveals a significant effect and interaction: $^{*}P < 0.05$; $^{\#}P < 0.01$ by Tukey's HSD test. (*C*) WB analyses for HDAC4 in nuclear and cytoplasmic fractions of 6-week-old mdx skeletal muscles. Gapdh and H3 were used as loading control of cytoplasmic and nuclear fractions, respectively. (*D*) Representative IF for HDAC4 in primary mdx myotubes. Scale bar: 20 μm. (*E*) Densitometric analysis of the WB bands for HDAC4, over Gapdh, in healthy and DMD patients' muscles. Gapdh was used as loading control. Data are expressed as mean ± SEM, over healthy subjects. n = 3 mice per condition. (*F*) HDAC activity assay in CTR, mdx, and mdx;KO GA muscles at 6 weeks of age. Data are expressed as mean ± SEM, over CTR muscles. n = 6 mice per condition. One-way ANOVA reveals a significant effect and interaction: $^{*}P < 0.05$; $^{\#}P < 0.01$ by Tukey's HSD test. (*G*) Real-time PCR for class II HDAC members in 6-week-old CTR, mdx, and mdx;KO mice. Data are presented as mean ± SEM, over CTR muscles. n = 4/5 mice for each genotype. One-way ANOVA reveals a significant effect and interaction: $^{*}P < 0.05$; $^{\#}P < 0.01$ by Tukey's HSD test.

fected muscle stem cell potential in mdx mice. Thus, we isolated SCs from mdx and mdx;KO mice and induced myogenic differentiation, assessed by IF for myosin heavy chain (MHC). Muscle cells isolated from mdx;KO mice showed significantly reduced differentiation and fusion abilities, as quantified by differentiation (i.e. the number of myonuclei

DOI: 10.1002/jcsm.12891

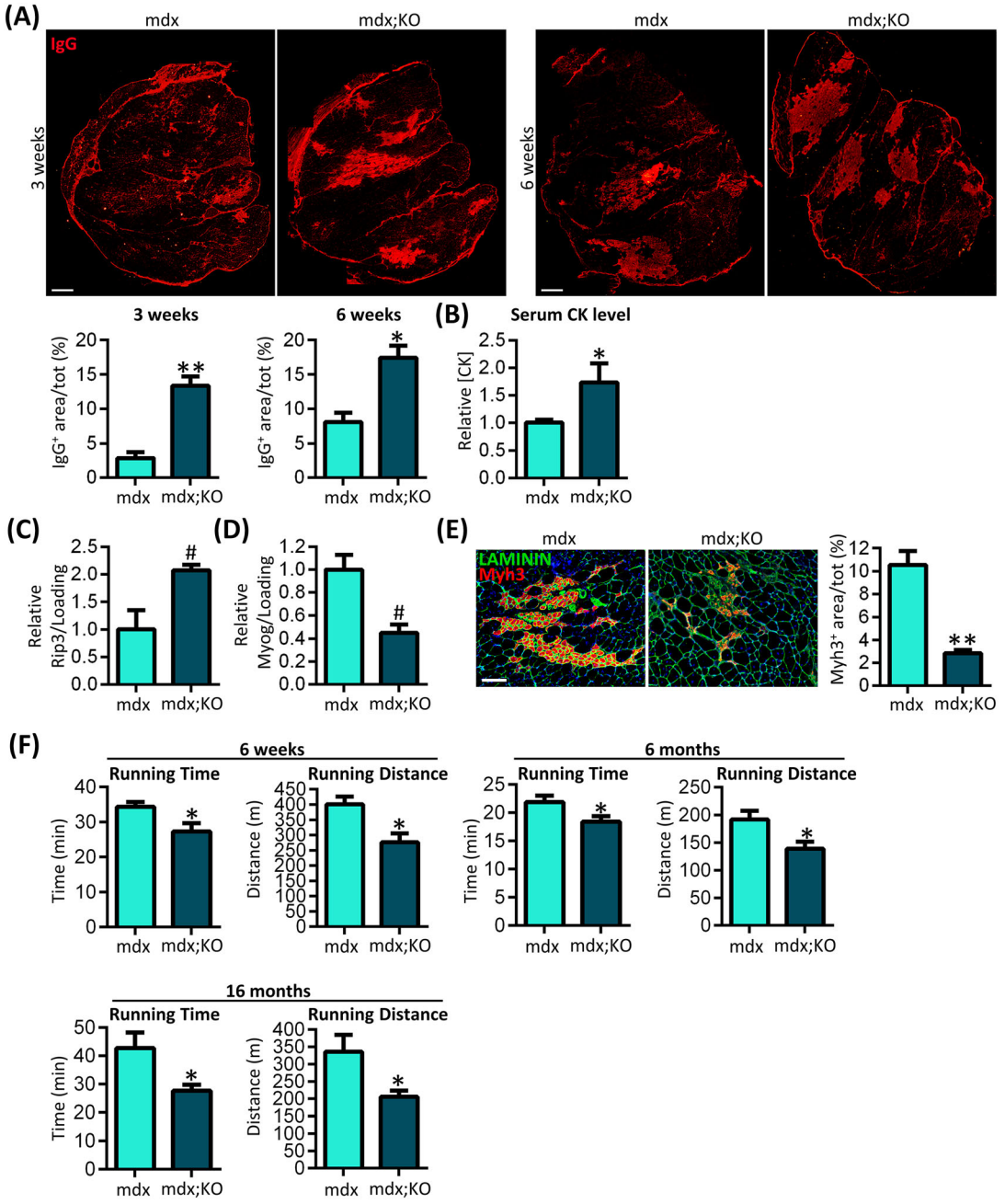

Figure 2 The deletion of HDAC4 in skeletal muscle exacerbates the pathological features of muscular dystrophy in mice. (*A*) Representative pictures of mdx and mdx;KO GA muscle labelled with IgG at 3 and 6 weeks of age. Scale bar: 500 μm. Quantification of the IgG-positive fibre CSA, over muscle CSA, of mdx and mdx;KO GA muscles at 3 and 6 weeks of age. Data are expressed as mean ± SEM. $n = 3$ mice per genotype, at each time point. $^{*}P < 0.05$; $^{**}P < 0.005$ by Student's *t*-test. (*B*) Creatine kinase levels in sera of mdx and mdx;KO mice at 6 weeks of age. Data are expressed as mean ± SEM, over mdx mice. $n = 7$ mice per genotype. $^{*}P < 0.05$ by Student's *t*-test. (*C*) Densitometric analyses of the WB bands for Rip3 protein in mdx and mdx;KO GA muscles, at 6 weeks of age. Stain-free protein bands were used as loading control. Data are shown as mean ± SEM, over mdx mice. $n = 3$ mice for each genotype. $^{\#}P < 0.01$ by Student's *t*-test. (*D*) Densitometric analyses of the WB bands for Myogenin protein in GA muscles of 6-week-old mdx and mdx;KO mice. Stain-free protein bands were used as loading control. Data are shown as mean ± SEM, over mdx mice. $n = 4/5$ mice for each genotype. $^{\#}P < 0.01$ by Student's *t*-test. (*E*) Representative IF for Myh3 (red) and laminin (green) in GA muscles of mdx and mdx;KO mice at 6 weeks of age and quantification of the Myh3-positive CSA. Scale bar: 100 μm. Data are expressed as mean ± SEM. $n = 3$ mice per genotype. $^{**}P < 0.005$ by Student's *t*-test. (*F*) Muscle performance of mdx and mdx;KO mice by treadmill test, at 6 weeks, 6 months, and 16 months. Data are presented as mean ± SEM. $n = 6$ mice per genotype. $^{*}P < 0.05$ by Student's *t*-test.

DOI: 10.1002/jcsm.12891

in MHC$^+$ cells over the total nuclei) and fusion (i.e. the number of myonuclei in myotubes over the total nuclei) indexes (*Figure* 3A). The decreased myogenic capacity of mdx;KO cells was corroborated by the lowered gene expression of the myogenic markers of terminal differentiation, that is, muscle creatine kinase (MCK) and myosins

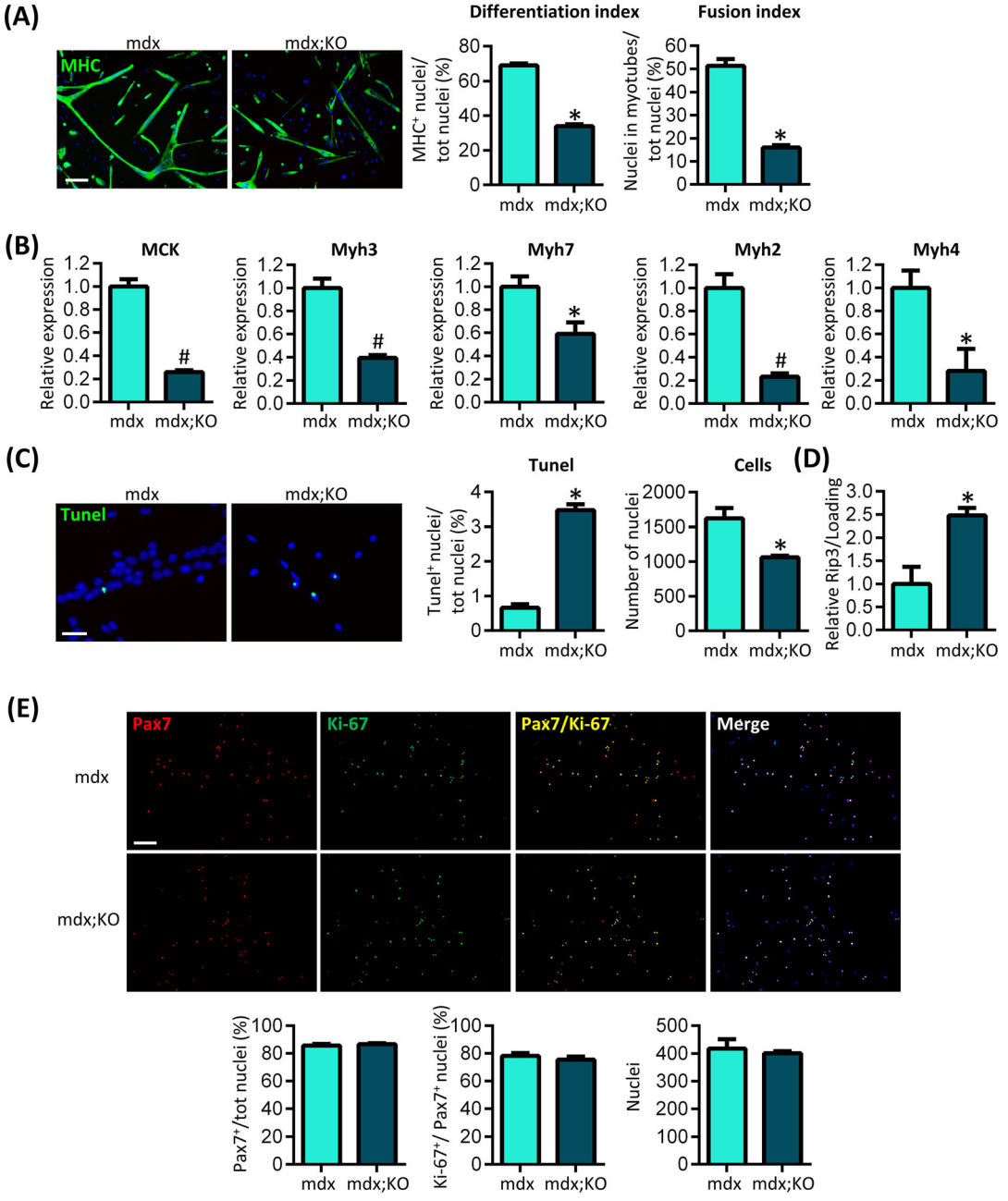

Figure 3 Mdx;KO muscle cells are not able to differentiate and are more susceptible to cell death. (*A*) Representative IF for MHC in mdx and mdx;KO primary muscle cells, after 3 days in differentiation medium. Scale bar: 100 μm. Quantification of differentiation and fusion indexes. Data are presented as mean ± SEM. n = 4 mice per genotype. *$P < 0.05$ mdx versus mdx;KO by Student's t-test. (*B*) Expression levels of terminal differentiation myogenic markers in mdx;KO muscle cells, over mdx ones, by real-time PCR. Data are presented as mean ± SEM. n = 4 mice per genotype. *$P < 0.05$; $^{\#}P < 0.01$ by Student's t-test. (*C*) Representative images of Tunel assay in mdx and mdx;KO primary muscle cells after 2 days of differentiation. Scale bar: 50 μm. Quantification of the Tunel-positive cells and number of muscle cells. Data are presented as mean ± SEM. n = 4 mice per genotype. *$P < 0.05$ mdx versus mdx;KO by Student's t-test. (*D*) Densitometric analyses of the WB bands for Rip3 protein in mdx and mdx;KO primary muscle cells. Stain-free protein bands were used as loading control. Data are shown as mean ± SEM, over mdx mice. n = 3 mice for each genotype. *$P < 0.05$ by Student's t-test. (*E*) Representative IF for Pax7 (red) and Ki-67 (green) in mdx and mdx;KO SCs. Scale bar: 100 μm. Quantification of Pax7-positive cells, Ki-67-positive SCs, and total number of isolated SCs. n = 3 mice per genotype.

DOI: 10.1002/jcsm.12891

Myh3, 7, 2, and 4, as measured by real-time PCR (*Figure* 3B).

Muscle cell survival was analysed by Tunel assay in differentiating cells: mdx;KO cells showed a significant increase in the Tunel-positive nuclei, compared with mdx cells, in parallel with a decrease in the overall number of nuclei (*Figure* 3C). Moreover, higher Rip3 levels were detected in differentiating mdx;KO muscle cells with respect to mdx ones (*Figures* 3D and S4A), indicating higher necroptosis occurring *in vitro* as well.

No significant differences in the number of $Pax7^+$ cells or $Ki67^+/Pax7^+$ cells were detected between mdx and mdx;KO samples (*Figure* 3E), indicating that SC proliferation was unaffected by HDAC4 deletion.

Importantly, skeletal muscle development and postnatal growth resulted unaffected in mdx;KO mice, with no significant differences in GA muscle total CSA or myofibre-CSA distribution at 2 weeks of age (*Figure* S4B), despite the deficit in muscle cell differentiation observed for the mdx;KO mice *in vivo* and *in vitro*.

Histone deacetylase 4 affects membrane stability and repair in mdx mice

To analyse muscle response to dystrophy-induced fragility, muscle damage was boosted by subjecting mdx mice to a downhill treadmill exercise at 6 months of age, at which point no significant differences between the genotypes were observed. Nonetheless, the quantification of EBD-positive area revealed not only that exercise increased muscle damage in dystrophic animals, as expected, but also that exercise-induced muscle damage was significantly higher in mdx;KO GA muscles compared with mdx ones (*Figure* 4A). Of note, neither CTR nor HDAC4mKO mice showed any sign of muscle necrosis upon treadmill, or differences in muscle performance (*Figure* S5), indicating the triggering of a specific function of HDAC4 in DMD.

Higher muscle permeability to the EBD may be a consequence of a defective membrane repair mechanism. Thus, we monitored the protein level and localization of two major players of this cellular response to damage, in the GA muscle of CTR, mdx, and mdx;KO mice at 6 weeks of age. A significant increase in Dysferlin and Trim72 protein levels was detected in mdx muscles, compared with CTR ones, as expected, while a reduction was observed in mdx;KO muscles, compared with mdx ones, by WB analysis (*Figures* 4B and S6A). Moreover, while both Dysferlin and Trim72 mainly localized in isolated dots in the proximity of the sarcolemma in mdx muscles, this pattern appeared altered in mdx;KO muscles by IF analyses (*Figure* 4C). In addition, Dysferlin and Trim72 protein levels and localization resulted induced and modulated in mdx myotubes as compared with CTR ones, while they were compromised in mdx;KO myotubes, compared with mdx ones (*Figures* 4D and 4E and S6B). Similar results were also observed in isolated myofibres (*Figure* S6C), further proving an involvement of HDAC4 in the membrane repair response.

Expression of Trim72 is sufficient to rescue the mdx;KO phenotype

Trim72 is an essential component of the cell membrane repair machinery and its knock-down results in compromised myoblast differentiation.[26] Considering that Trim72 was reduced in mdx;KO myotubes, we hypothesized that enhanced membrane damage due to lack of Trim72 underpinned the reduced myofibre survival and the impaired muscle cell differentiation in mdx;KO mice. To test this hypothesis out, we restored Trim72 expression by transfecting a c-myc-tagged Trim72-expressing plasmid, or a GFP-expressing plasmid as control, in mdx;KO muscle cells. Preliminary experiments demonstrated that the overexpression of pCDNA3-N2myc or GFP plasmid did not affect mdx;KO cell differentiation (data not shown). Also, we confirmed the Trim72 overexpression by real-time PCR (*Figure* 5A). When we analysed the mdx;KO cell myogenic potential, we noted that Trim72 significantly improved mdx;KO cell ability to differentiate, as quantified by fusion index and by the expression levels of MCK and Myh3 genes (*Figure* 5B and 5C). Moreover, expression of Trim72 led to a significant decrease in the Tunel-positive nuclei, in parallel with an increase in the number of transfected mdx;KO cells compared with controls (*Figures* 5D and S7A). Taking into account that Trim72 overexpression promotes mdx;KO cell survival, our findings indicate that (1) higher cell death may be the cause of the reduced ability of mdx;KO muscle cells to differentiate; (2) preserving the membrane repair mechanism promotes mdx;KO muscle cell differentiation. Importantly, ectopic expression of Dysferlin in mdx;KO muscle cells did not improve their fusion or number (*Figure* S7B and S7C), indicating a specific function of Trim72 in the rescue of the mdx;KO phenotype.

To further prove the involvement of HDAC4-dependent pathways in mediating the membrane repair mechanism response *in vivo*, we electroporated c-myc-tagged Trim72-expressing plasmid, or GFP-expressing plasmid as control, in mdx;KO GA muscles, at 5.5 months of age. First, we confirmed the efficiency in gene delivery and the resulting Trim72 up-regulation by WB analyses and IF for c-myc or GFP (*Figures* 5E and S8A and S8B). Two weeks after the electroporation, mice were subjected to the downhill exercise protocol to induce muscle damage, as performed for the previous experiments, and the muscle phenotype was evaluated, in terms of muscle morphology, necrosis, and functionality. Expression of Trim72 visibly decreased muscle necrosis and ameliorated mdx;KO muscle morphology, as evidenced by H&E staining (*Figure* 5F). In addition, the quantification of

DOI: 10.1002/jcsm.12891

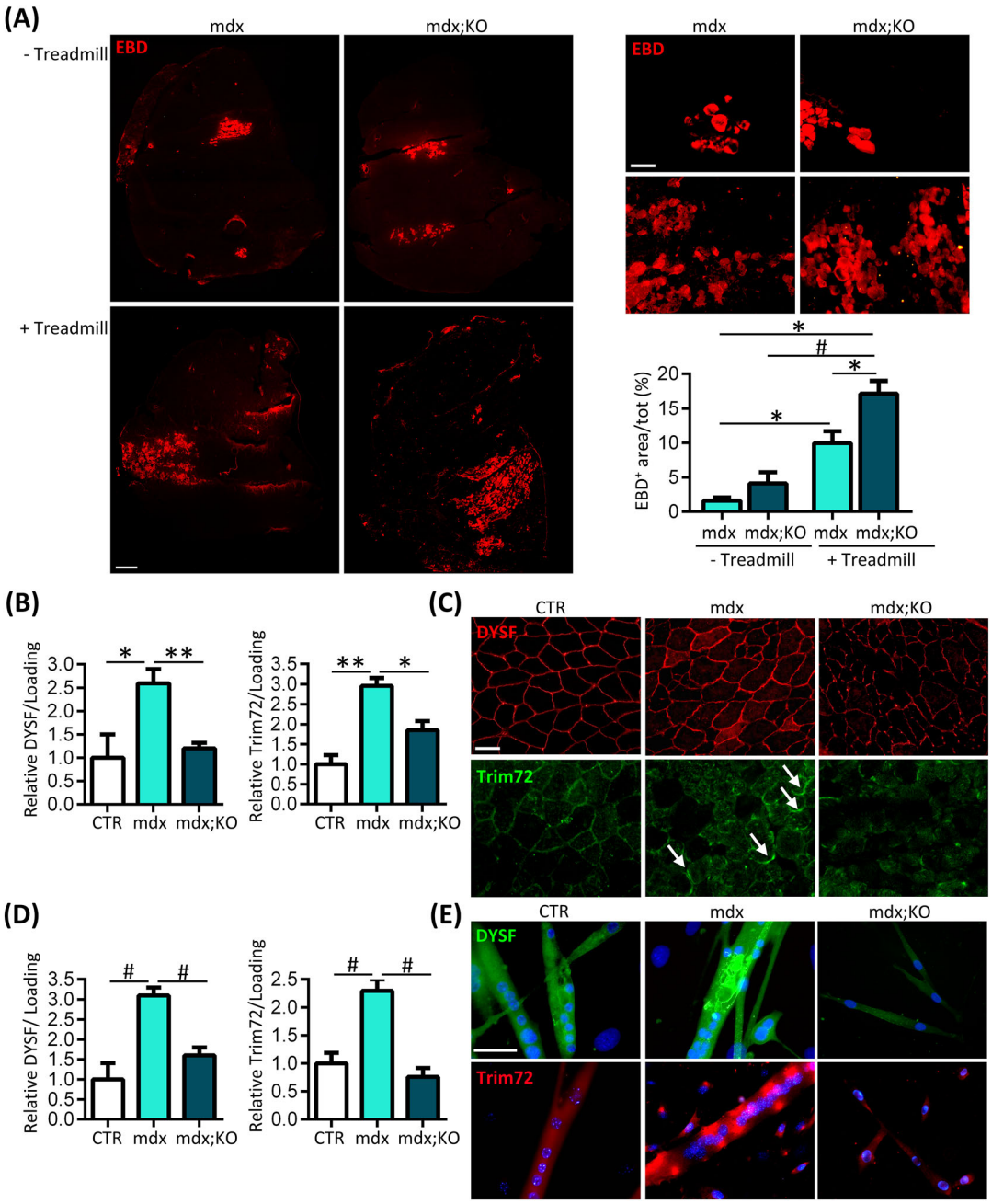

Figure 4 HDAC4 affects membrane stability and is necessary for an adequate expression and localization of proteins involved in the membrane repair mechanism in mdx mice. (*A*) Representative images of mdx and mdx;KO GA muscle at 6 months of age with or without treadmill exercise, labelled with EBD and quantification of EBD-positive fibre CSA, over muscle CSA. Scale bars: 500 and 100 μm. Data are expressed as mean ± SEM. n = 5 mice per genotype. Two-way ANOVA reveals a significant effect and interaction: $^{*}P < 0.05$; $^{\#}P < 0.01$ by Tukey's HSD post hoc test. (*B*) Densitometric analyses of the WB bands for Dysferlin and Trim72 proteins in CTR, mdx, and mdx;KO GA muscles, at 6 weeks of age. Stain-free protein bands were used as loading control. Data are shown as mean ± SEM, over mdx mice. n = 3–6 mice for each genotype. One-way ANOVA reveals a significant effect and interaction: $^{*}P < 0.05$; $^{**}P < 0.005$ by Tukey's HSD post hoc test. (*C*) Representative images of CTR, mdx, and mdx;KO GA muscle at 6 weeks of age, labelled with Dysferlin (red) or Trim72 (green). Scale bar: 100 μm. (*D*) Densitometric analyses of the WB bands for Dysferlin and Trim72 proteins in CTR, mdx, and mdx;KO primary muscle cells. Stain-free protein bands were used as loading control. Data are shown as mean ± SEM, over mdx mice. n = 3–6 mice for each genotype. One-way ANOVA reveals a significant effect and interaction: $^{\#}P < 0.01$ by Tukey's HSD post hoc test. (*E*) Representative images of CTR, mdx, and mdx;KO differentiated primary muscle cells labelled with Dysferlin (green) or Trim72 (red). Scale bar: 50 μm.

DOI: 10.1002/jcsm.12891

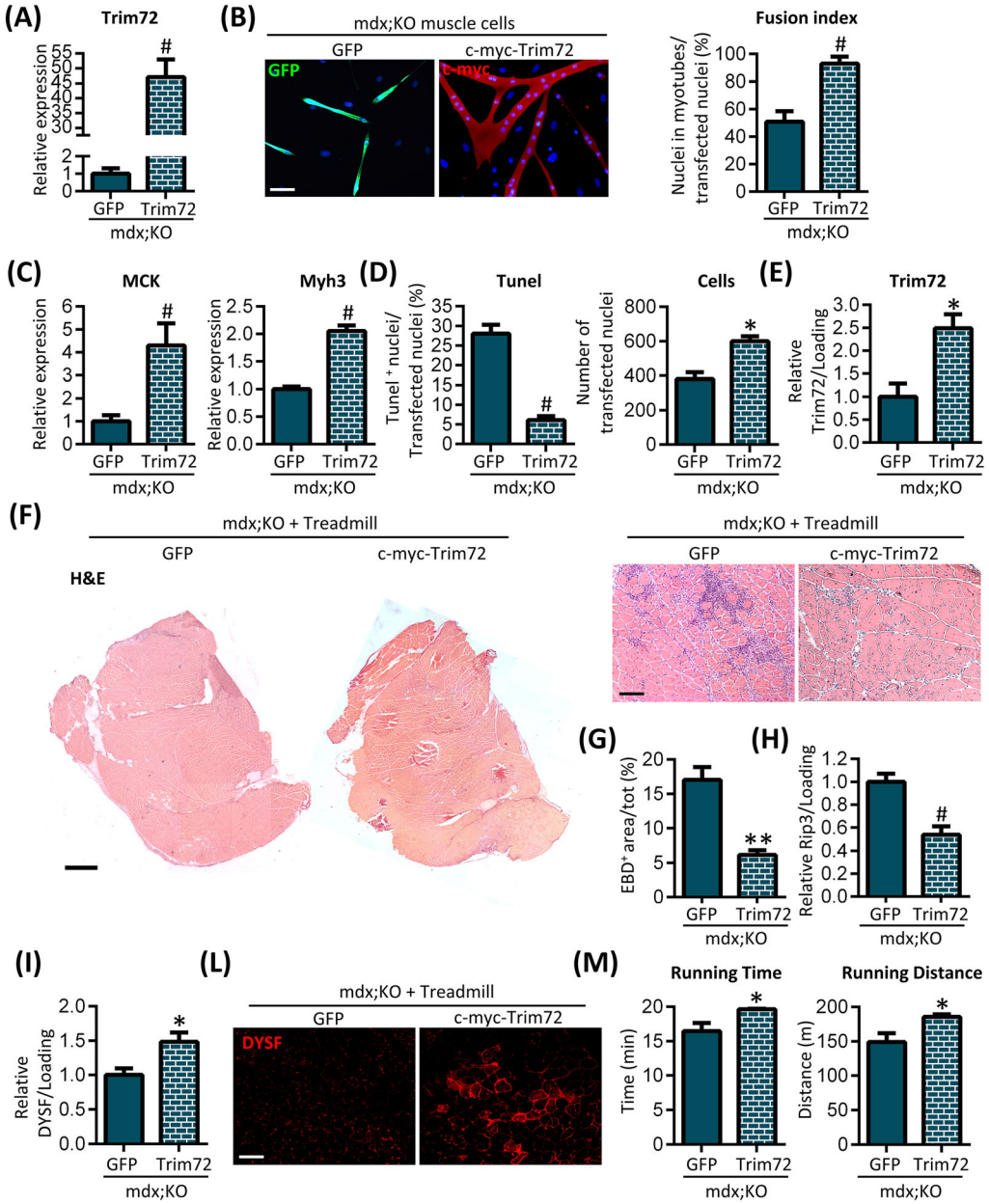

Figure 5 The ectopic expression of Trim72 is sufficient to rescue mdx;KO phenotype *in vitro* and *in vivo*. (*A*) Trim72 expression in mdx;KO muscle cells transfected with Trim72-expressing plasmid, over GFP-transfected ones, by real-time PCR. Data are presented as mean ± SEM. $n = 4$ mdx;KO mice. $^{\#}P < 0.01$ by Student's *t*-test. (*B*) Representative IF for GFP or c-myc in mdx;KO cells transfected with either GFP or c-myc-Trim72 after 3 days of differentiation. Scale bar: 50 μm. Quantification of fusion index. Data are presented as mean ± SEM. $n = 4$ mdx;KO mice. $^{\#}P < 0.01$ by Student's *t*-test. (*C*) Expression levels of myogenic markers in c-myc-Trim72 mdx;KO transfected muscle cells, over GFP transfected ones, by real-time PCR. Data are presented as mean ± SEM. $n = 4$ mice per genotype. $^{\#}P < 0.01$ by Student's *t*-test. (*D*) Quantification of the Tunel-positive cells and number of mdx;KO cells transfected with either GFP or c-myc-Trim72 after 2 days of differentiation. Data are presented as mean ± SEM. $n = 3$ mdx;KO mice. $^{*}P < 0.05$; $^{\#}P < 0.01$ by Student's *t*-test. (*E*) Densitometric analyses of the WB bands for Trim72 levels in mdx;KO GA muscles electroporated with either Trim72-expressing plasmid or GFP, as control, by WB analysis. Stain-free protein bands were used as loading control. Data are shown as mean ± SEM, over GFP-electroporated muscles. $n = 4/5$ muscles per condition. $^{*}P < 0.05$ by Student's *t*-test. (*F*) Representative images of mdx;KO GA muscles electroporated with either c-myc-Trim72-expressing plasmid or GFP, as control, stained with haematoxylin and eosin. Scale bars: 500 and 100 μm. (*G*) Quantification of the EBD-positive fibre CSA, over muscle CSA. Data are expressed as mean ± SEM. $n = 4$ mice per condition. $^{**}P < 0.005$ by Student's *t*-test. (*H*) Densitometric analyses of the WB bands for Rip3 protein in mdx;KO GA electroporated muscles. Stain-free protein bands were used as loading control. Data are shown as mean ± SEM, over GFP-electroporated muscles. $n = 4$ muscles per condition. $^{\#}P < 0.01$ by Student's *t*-test. (*I*) Densitometric analyses of the WB bands for Dysferlin protein in mdx;KO GA electroporated muscles. Stain-free protein bands were used as loading control. Data are shown as mean ± SEM, over GFP-electroporated muscles. $n = 4$ muscles per condition. $^{*}P < 0.05$ by Student's *t*-test. (*L*) Representative IF for Dysferlin (DYSF) in mdx;KO GA electroporated muscles. Scale bar: 100 μm. (*M*) Muscle performance of mdx;KO mice electroporated with either c-myc-Trim72 expressing vector or GFP by treadmill test. Data are presented as mean ± SEM. $n = 4$ mice per condition. $^{*}P < 0.05$ by Student's *t*-test.

DOI: 10.1002/jcsm.12891

EBD-positive fibres proved that delivery of Trim72 significantly reduced the area of damaged fibres in mdx;KO muscles, with respect to controls (*Figures* 5G and S8C). A decrease in muscle necroptosis was demonstrated by WB analyses for Rip3 protein levels, which resulted significantly reduced in the Trim72-electroporated mdx;KO muscles, compared with controls (*Figures* 5H and S8D). Moreover, Trim72 expression was sufficient to restore Dysferlin protein levels and localization in mdx;KO muscles, as proved by WB and IF analyses (*Figures* 5I and 5L and S8D), in line with a previous study.[27] Importantly, mdx;KO mice electroporated with Trim72 ran a significantly longer time and distance than the relative controls (*Figure* 5M). The comparison with the age-matched mdx mice (*Figure* 2F) revealed no major differences between mdx and Trim72-electroporated mdx;KO mice as to both the parameters, indicating that Trim72 overexpression was sufficient for the full functional rescue of the deficit induced by the deletion of HDAC4.

Expression of cytoplasmic-restricted histone deacetylase 4 improves the mdx;KO phenotype

Because HDAC4 is mainly localized in the cytoplasm in adult mdx muscles and considering that mdx;KO SCs suppress HDAC4 expression after myogenin is expressed, that is, during their differentiation, we speculated that the deficit in mdx;KO muscle cell differentiation and survival depended on a cytoplasmic function of HDAC4. To verify this hypothesis, we overexpressed the GFP-tagged wild-type HDAC4, the nuclear-restricted HDAC4-3SA mutant,[2,28] and the cytoplasmic-restricted GFP-tagged HDAC4-L175A mutant[2] in proliferating mdx;KO muscle cells. Then both these cells and cells transfected with the GFP-expressing plasmid, used as a control, were induced to differentiate. Gene delivery efficiency was quantified by real-time PCR for *Hdac4* in transfected cells (*Figure* 6A). While the wild-type HDAC4 or the nuclear one did not improve mdx;KO muscle cell differentiation, the expression of the cytoplasmic HDAC4 (HDAC4 L/A) strongly increased mdx;KO cell fusion and cell number (*Figure* 6A). These results did not correlate with the levels of expression of the different constructs. This implies that the difference in HDAC4 constructs (resulting in differential HDAC4 localization), rather than the difference in their expression levels, was solely responsible for the results. Indeed, an increase of the fusion index correlates with increased nuclear density, as observed in HDAC4 L/A overexpressing mdx;KO cells, pointing to the importance of preserving cell survival to favour myoblast fusion.

Based on these encouraging data with cell cultures, we electroporated GFP-tagged HDAC4-L175A-expressing plasmid, or the GFP-expressing plasmid, in the mdx;KO GA, at 5.5 months of age, to validate the effects of cytoplasmic HDAC4 expression *in vivo*. Two weeks after the electroporation, mice were subjected to the muscle damage-inducing downhill exercise protocol. The muscle phenotype was subsequently evaluated, in terms of muscle necrosis, regeneration, and function. Expression of cytoplasmic HDAC4 apparently decreased necrosis and improved regeneration in mdx;KO muscles, compared with controls, by H&E staining (*Figure* 6B). Gene delivery efficiency was determined by quantifying HDAC4 protein levels by WB analyses and by IF for GFP (*Figures* 6C and S9A and S9B). A more detailed evaluation of the EBD-positive fibres proved that delivery of cytoplasmic HDAC4 significantly reduced the extent of necrotic area in mdx;KO muscles, with respect to controls (*Figures* 6D and S9C). Decrease in muscle necroptosis was further demonstrated by WB analyses for Rip3 protein levels, which resulted significantly reduced in the HDAC4 L/A-electroporated mdx;KO muscles, compared with the GFP-electroporated ones (*Figures* 6E and S10A). Increased muscle regeneration was confirmed by the observed higher levels of myogenin and Myh3 proteins in HDAC4 L/A-electroporated muscles, with respect to controls (*Figures* 6F, S9B, and S10B). Notably, the expression of cytoplasmic HDAC4 induced the higher expression of Dysferlin and Trim72 proteins (*Figures* 6G and S9B), likely resulting in highly efficient membrane repair. Consistently with all of the above, mdx;KO mice electroporated with HDAC4 L/A ran for a significantly longer time and distance than those electroporated with GFP-expressing plasmid (*Figure* 6H).

Overall, these data clearly indicate that the protective role of HDAC4 in mediating membrane stability and muscle regeneration in DMD relies on a cytoplasmatic function.

The protective role of cytoplasmic histone deacetylase 4 is partially independent of its deacetylase activity and may involve mRNA stability in Duchenne muscular dystrophy

To further investigate the molecular mechanisms dependent on HDAC4 in DMD, we wondered whether the cytoplasmic functions of HDAC4 require its deacetylase activity. A GFP-tagged cytoplasmic-restricted and catalytically dead double-mutant form of HDAC4 was obtained by an asparagine (N) for aspartic acid (D) substitution in its active site (D840N)[29] in conjunction with the mutation of the NLS sequence; this construct was expressed in mdx;KO muscle cells and compared with GFP-HDAC4, GFP-HDAC4 L/A, and GFP (used as a control). Skeletal muscle cell differentiation was then analysed to assess whether the deacetylase activity of HDAC4 is required to exert its function. Expression of the mutant HDAC4 L/A D840N greatly increased mdx;KO cell fusion and cell number (*Figure* 7A), although to a lesser extend if compared with GFP-HDAC4 L/A overexpression, indicating that the protective function of HDAC4 in mdx;KO cells is partially independent of its deacetylase activity.

DOI: 10.1002/jcsm.12891

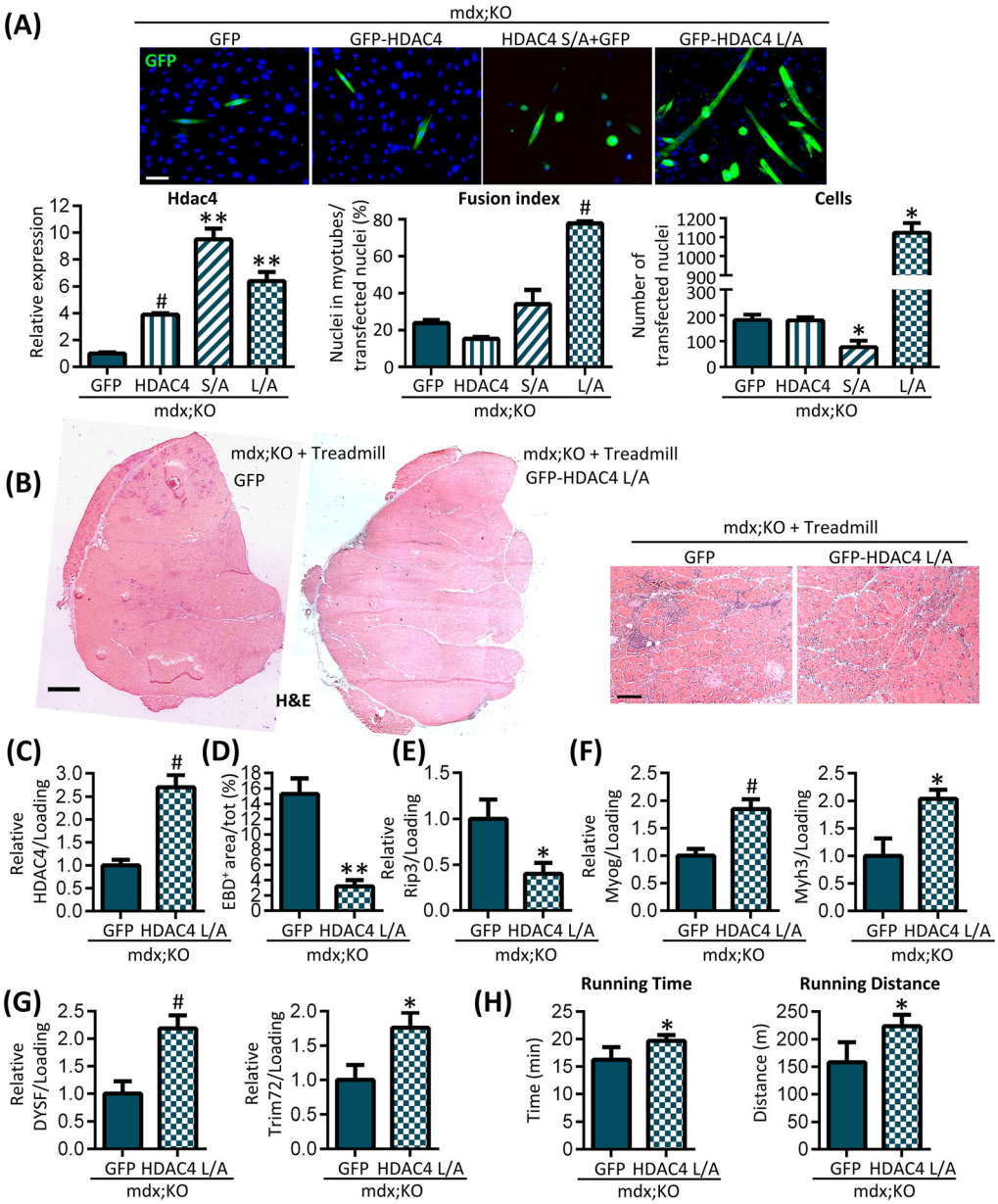

Figure 6 The ectopic expression of cytoplasmic-restricted HDAC4 ameliorates mdx;KO phenotype *in vitro* and *in vivo*. (*A*) Representative IF for GFP in mdx;KO primary muscle cells transfected with GFP, GFP-HDAC4, HDAC4 S/A + GFP, or GFP-HDAC4 L/A after 3 days of differentiation. Scale bar: 50 μm. HDAC4 expression in mdx;KO muscle cells transfected with GFP-HDAC4 or HDAC4 S/A + GFP or GFP-HDAC4 L/A expressing plasmid, over GFP-transfected ones, by real-time PCR. Data are presented as mean ± SEM. n = 3 mdx;KO mice; $^{**}P < 0.005$; $^{\#}P < 0.01$ versus GFP-transfected cells by Student's t-test. Quantification of fusion index and number of muscle cells. n = 3 mdx;KO mice. Data are presented as mean ± SEM. $^{*}P < 0.05$; $^{\#}P < 0.01$ versus GFP-transfected cells by Student's t-test. (*B*) Representative images of mdx;KO GA muscles electroporated with either HDAC4 L/A expressing vector or GFP, as control, stained with H&E. Scale bars: 500 and 100 μm. (*C*) HDAC4 expression in mdx;KO GA muscles electroporated with either HDAC4 L/A expressing plasmid or GFP, as control, by WB analysis. Stain-free protein bands were used as a loading control. Data are shown as mean ± SEM, over GFP-electroporated muscles. n = 4/5 muscles per condition. $^{\#}P < 0.01$ by Student's t-test. (*D*) Quantification of EBD-positive fibre CSA, over muscle CSA, in electroporated mdx;KO muscles. Data are expressed as mean ± SEM. n = 4/5 mice per condition. $^{**}P < 0.005$ by Student's t-test. (*E*) Densitometric analyses of the WB bands for Rip3 protein in mdx;KO GA electroporated muscles. Stain-free protein bands were used as a loading control. Data are expressed as mean ± SEM, over GFP-electroporated muscles. n = 4 mice per condition. $^{*}P < 0.05$ by Student's t-test. (*F*) Densitometric analyses of the WB bands for Myogenin and Myh3 protein levels in mdx;KO GA electroporated muscles. Stain-free protein bands were used as a loading control. Data are shown as mean ± SEM, over GFP-electroporated muscles. n = 4/5 muscles per condition. $^{*}P < 0.05$; $^{\#}P < 0.01$ by Student's t-test. (*G*) Densitometric analyses of the WB bands for Dysferlin and Trim72 protein levels in mdx;KO GA electroporated muscles. Stain-free protein bands were used as a loading control. Data are shown as mean ± SEM, over GFP-electroporated muscles. n = 4 muscles per condition. $^{*}P < 0.05$; $^{\#}P < 0.01$ by Student's t-test. (*H*) Muscle performance of mdx;KO mice electroporated with either HDAC4 L/A expressing vector or GFP, as control, by treadmill test. Data are presented as mean ± SEM. n = 4/5 mice per condition. $^{*}P < 0.05$ by Student's t-test.

DOI: 10.1002/jcsm.12891

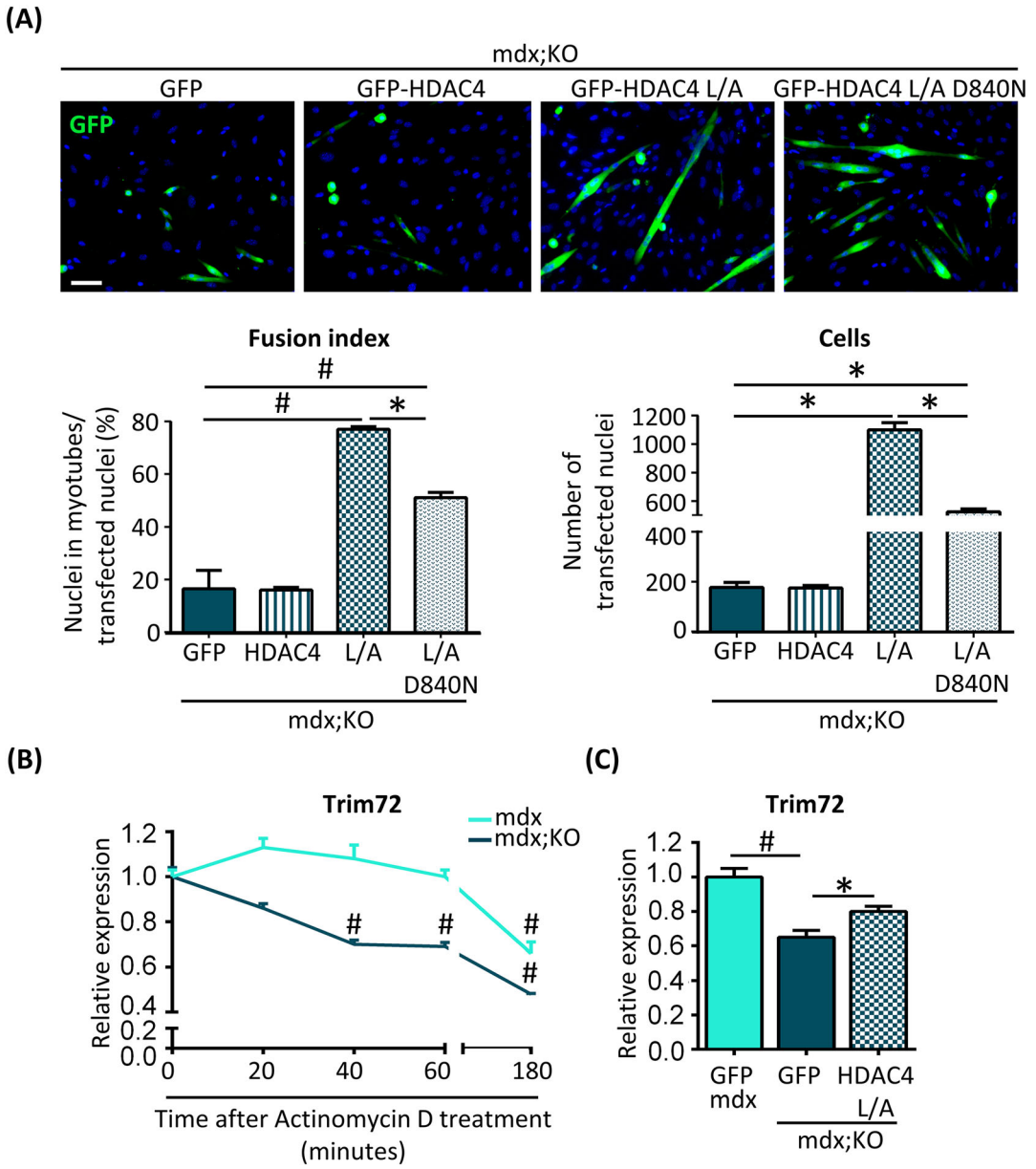

Figure 7 HDAC4 modulates Trim72 mRNA stability in mdx satellite cells. (*A*) Representative IF for GFP in mdx;KO primary muscle cells transfected with GFP-HDAC4, GFP-HDAC4 L/A, GFP-HDAC4 L/A D840N, or GFP-expressing plasmids and terminally differentiated. Scale bar: 50 μm. Quantification of the fusion index and number of muscle cells. Data are presented as mean ± SEM. n = 3 mdx;KO mice. One-way ANOVA reveals a significant effect and interaction: $^{*}P < 0.05$; $^{\#}P < 0.01$ by Tukey's HSD post hoc test. (*B*) Real-time PCR analyses of transcript levels of Trim72 in mdx (light blue) and mdx;KO (dark blue) myotubes treated with Actinomycin D. The relative expression of Trim72 at different time points was calculated by normalizing the gene expression in Actinomycin D-treated mdx or mdx;KO samples over untreated samples (t = 0). Data are presented as mean ± SEM. n = 3. One-way ANOVA reveals a significant effect: $^{\#}P < 0.01$ mdx or mdx;KO-treated samples versus t = 0 by Tukey's HSD test. (*C*) Expression levels of Trim72 in mdx;KO transfected muscle cells with GFP or GFP-HDAC4 L/A, over mdx SCs, by real-time PCR. Data are presented as mean ± SEM. n = 3 mice per genotype. One-way ANOVA reveals a significant effect and interaction: $^{*}P < 0.05$; $^{\#}P < 0.01$ by Tukey's HSD test.

In search for a cytoplasmic function of HDAC4, we initially hypothesized that it could act as a scaffold or docking chaperone for Trim72, on the basis of a possible interaction between HDAC4 and Trim72 proteins. Co-IP experiments demonstrated that c-myc-Trim72 does not interact with HDAC4 in primary mdx myotubes (*Figure* S11A), excluding a direct interaction between these two proteins. However, because Trim72 expression directly correlates with that of HDAC4, we speculated that HDAC4 may control Trim72 expression by stabilizing its mRNA. To test this hypothesis,

DOI: 10.1002/jcsm.12891

mdx;KO and mdx terminally differentiated myotubes were treated with a RNA polymerase inhibitor, that is, ActD. Total RNA was collected at different time points of ActD treatment, then Trim72 mRNA levels were analysed by real-time PCR. As a control for the effectiveness of the treatment, the c-myc mRNA level was assessed in mdx;KO and mdx-treated myotubes, showing the expected, time-dependent decrease for a given RNA independently of the genotype (*Figure* S11B). While in mdx myotubes, Trim72 mRNA levels were stable for at least 60 min following ActD treatment, in mdx;KO myotubes, Trim72 mRNA levels were significantly lower after 40 min of ActD treatment (*Figure* 7B). Interestingly, Trim72 mRNA levels correlated with HDAC4 expression in dystrophic myotubes, being both lower in mdx;KO cells compared with mdx cells and significantly higher upon expression of the cytoplasmic-restricted HDAC4 (*Figure* 7C). Taken together, these data suggest the involvement of HDAC4 in the maintenance of the Trim72 mRNA level in dystrophic myotubes.

Discussion

DMD is a devastating genetic disorder, caused by numerous mutations in the X-linked *DMD* gene, which encodes a structural protein in skeletal muscle that connects the intracellular cytoskeleton to the extracellular matrix.[11] DMD patients manifest deambulatory problems and muscle weakness in the first few years of life, and the progressive degeneration of their skeletal muscle forces them in a wheelchair from early adolescence. This disease progresses causing skeletal deformities, cardiomyopathy, and respiratory insufficiency, ultimately leading to the death of patients between 30 and 40 years of age.[11]

Since the discovery of the *DMD* gene, numerous different therapeutic approaches have been proposed to counteract DMD progression and improve muscle function. Among them, oligonucleotide-mediated exon skipping, gene replacement (to provide truncated forms of dystrophin), and stem cell therapy have produced promising results in preclinical trials, and some of them have reached the clinical trial stage.[30] Recently, the new genetic tool based on the CRISPR (Clustered Regularly Interspaced Short Palindromic Repeats)/Cas9 system gave new hope for DMD treatment, restoring dystrophin expression in both the germline and postnatal tissues of mdx mice. Despite the promising results of these newly developed strategies of gene editing, there are several important constraints to be considered for future clinical trials. First, the low efficiency of gene delivery to all muscles and the heart and, secondly, the extremely expensive large-scale production of the viral particles needed for the patients. Moreover, it is not known how long this amended dystrophin expression in edited cells lasts, if the Cas9 long-term expression in the body is going to lead to side effects, what the possible risk of off-target mutations in the genome caused by gene editing *in vivo* is.

Differently from gene therapy, pharmacological approaches target the downstream effects caused by *DMD* mutations, preventing DMD progression. Promoting membrane repair mechanism[14] or muscle regeneration[31] are two of the most desirable goals to slow down muscle dystrophy. In this scenario, pan-HDACi have been proposed for the treatment of DMD due to their ability to promote the morphological and functional recovery of dystrophic muscles in preclinical studies, favouring muscle regeneration at the expense of fibro-adipogenic degeneration.[15] However, in a phase II clinical study with the pan-HDACi givinostat, no functional recovery was reported and no definitive conclusion could be drawn because of the limited sample size.[16] Moreover, treatment with pan-HDACi proved inefficient in adult dystrophic mice,[15] and long-term treatment with HDACi, as required for DMD, was associated with numerous side effects,[17] raising additional concerns about proposing pan-HDACi as a pharmacological therapy. Most of these limits may be due to the broad action of the pan-HDACi, considering that different classes of HDAC play different functions and some of them may be beneficial in DMD. The identification, therefore, of the specific functions of different HDAC classes represents a prerequisite for proposing more specific compounds or combined approaches, which may improve the effectiveness of DMD treatments.

With this rationale, we decided to clarify the pathways modulated by HDAC4 in DMD. We found the expression of HDAC4 to be up-regulated in muscles of mdx mice and, of note, of DMD patients' muscles compared with healthy muscles, in spite of a great variability in these results. The low number of human samples available (n = 3) and the differential mutations in the *DMD* gene (e.g. the frameshift in the exons 45–50 is generally associated with a milder DMD phenotype) may result in the different levels of severity of the phenotype, while the corticosteroid treatment (administered to one patient) may further account for the variability observed. Of note, the highest level of HDAC4 protein is present in the muscle of the patient presenting a mutation associated with a more severe DMD phenotype and who was taking no pharmacological treatment. This is the first direct evidence of an elevated expression of HDAC4 in the musculature of DMD patients.

We also found that the activity of class IIa, of class I, and of class I/IIb HDACs was up-regulated in mdx mice. Previously published data reported the up-regulation of HDAC4 in several diseases, such as in amyotrophic lateral sclerosis (ALS)[7] or cancer,[32] and this is the reason why HDAC4 inhibition was proposed as potential treatment for these pathologies. However, we proved that HDAC4 inhibition in cases of long-term denervation or in ALS is detrimental for skeletal muscle homeostasis.[6,7] These unpredicted results may be a

consequence of the genetic deletion of HDAC4 before the onset of the diseases; nonetheless, they indicate that HDAC4 up-regulation is needed in skeletal muscle to properly respond to stress.

We also found that HDAC4 prevalently localizes in the cytoplasm of mdx muscles, probably due to an imbalance of the calcium influx and the reduced NO-dependent protein phosphatase 2A activity.[10] Recent findings are challenging the notion that cytoplasmic HDAC4 is simply an inactive epigenetic factor, at least in skeletal muscle. For instance, HDAC4 has been demonstrated to promote the deacetylation of specific cytosolic substrates, thereby regulating muscle atrophy and metabolism.[3] We therefore hypothesized that HDAC4 plays a pivotal role in the cytosol of skeletal muscle in response to the stress associated with the lack of dystrophin. Indeed, dystrophic mice with skeletal muscle-specific HDAC4 deletion showed higher muscle damage, accompanied with reduced muscle regeneration, due to increased myoblast death and the impaired ability of muscle cells to differentiate. Importantly, HDAC4 deletion in skeletal muscle *per se* does not affect the myogenic potential of muscle cells,[9] indicating a specific HDAC4 function in the absence of dystrophin.

Overall muscle functionality resulted compromised in young, adult, and elderly mdx;KO mice, compared with mdx littermates, indicating that HDAC4 deletion severely affects mdx mice of all ages. In particular, the running distance dropped more conspicuously than the running time, suggesting that both the running speed and the resistance to fatigue were affected by HDAC4 deletion.

In the absence of dystrophin, the sarcolemma is more fragile, thus more prone to contraction-induced damage. The deletion of HDAC4 sensitizes mice to dystrophic abnormalities, enhancing muscle fragility. This phenomenon is strictly related to the dystrophic condition, because mice with muscle-specific HDAC4 deletion alone did not show muscle damage or functional deficit following treadmill exercise.

One of the principal mechanisms triggered by damage in skeletal muscle membrane is its repair mechanism, which is normally up-regulated in dystrophic conditions and accounts, at least initially, for proper muscle homeostasis.[14,33] Consistently, Trim72 levels increase in mdx skeletal muscles and sera, compared with wild-type mice,[14] as happens in DMD patients' skeletal muscles.[34] We also found an aberrant response of the membrane repair mechanism in mdx;KO mice, both *in vivo* and *in vitro*, which probably underpins the higher membrane fragility and the reduced myogenic potential of mdx;KO muscle cells. The lack of dystrophin negatively affects SC capacity to contribute to muscle regeneration.[35] We expanded this notion with the evidence that, together with the absence of dystrophin, the lack of HDAC4 further hampers SC myogenic potential. As a matter of fact, most of the proteins involved in the membrane repair mechanism are important for proper myoblast fusion and to maintain myogenic potential.[26,36] From our data, a defective membrane repair mechanism leads to higher cell death together with compromised muscle cell differentiation and higher muscle necrosis *in vivo*. Indeed, the ectopic expression of Trim72 restores mdx;KO muscle cell survival and myogenic potential *in vitro*, also improving muscle function *in vivo*. All of the above generates a model whereby in muscle tissue, HDAC4 is needed to activate the membrane repair response caused by the lack of dystrophin, synergistically contributing with dystrophin to the maintenance to muscle homeostasis. Differently from Trim72, the ectopic expression of Dysferlin does not improve mdx;KO muscle cell fusion or survival; instead, it reduces the number of mdx;KO muscle cells. Our results are in line with previous studies showing that the overexpression of Trim72 facilitates sarcolemma repair in response to multiple insults, including muscle dystrophy,[14] while Dysferlin overexpression is detrimental for murine skeletal muscle.[37] Also, defects in the membrane repair mechanism associated with mutations in Trim72 are not rescued by Dysferlin overexpression,[33] in-

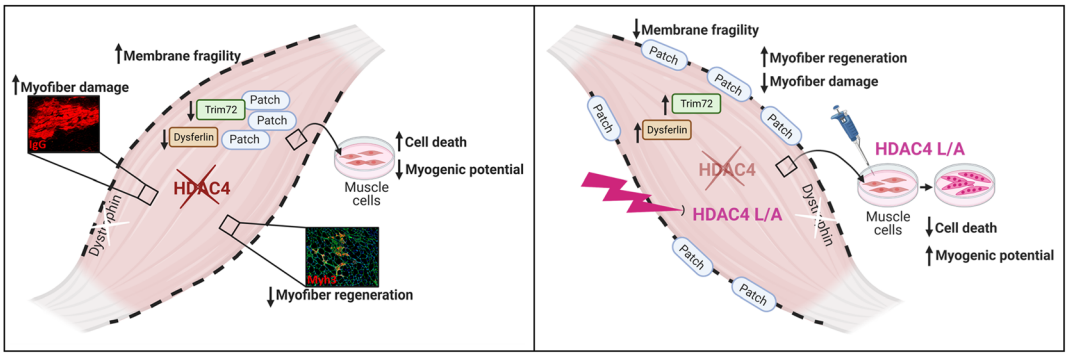

Figure 8 Model of the proposed role of HDAC4 in DMD muscles. Cytoplasmic HDAC4 mediates the membrane repair mechanism response, thus promoting muscle stem cell survival and fusion *in vitro*, restoring muscle integrity, and favouring de novo myogenesis *in vivo*. Taken together, these functions result in improved muscle architecture and function in mdx mice.

DOI: 10.1002/jcsm.12891

dicating that these two proteins have specific functions. Importantly, the ectopic expression of Trim72 is sufficient to restore Dysferlin protein levels and to protect skeletal muscle from apoptosis and damage in a muscular dystrophy hamster model,[27] suggesting that Trim72 may be administered as a possible treatment for DMD.[14] Nevertheless, some important safety concerns have been reported about the long-term delivery of Trim72. In one study, by using the non-specific cytomegalovirus promoter to drive Trim72 expression so as to improve muscular dystrophy, severe growth retardation was observed in hamster neonates, suggesting a potential toxicity due to its overexpression in non-muscle tissues, especially the liver.[27] In addition, the overexpression of Trim72 in striated muscles resulted in metabolic disorder and diabetic cardiomyopathy,[38,39] due to its E3-ubiquitin ligase functions that alter the insulin pathway.[38,40]

We proved that the expression of HDAC4 in cytoplasm correlates with the onset of the membrane repair mechanism response *in vitro*, promoting muscle stem cell survival and fusion, and *in vivo*, ameliorating muscle fragility, promoting *de novo* myogenesis, and improving overall muscle function in mdx;KO mice. Enhanced muscle regeneration in HDAC4 L/A-electroporated mdx;KO muscles suggests that there exists a HDAC4 pro-regenerative function independent of Trim72 pathway in dystrophic skeletal muscle, possibly related to autocrine/paracrine functions of HDAC4.[9] No significant differences were instead observed in pre-synaptic and post-synaptic NMJ terminals between mdx and mdx;KO muscles (*Figure* S12) that may account for impaired fibre maturation and compromised regeneration.

These findings point to the need to deliver the cytoplasmic-restricted form of HDAC4, instead of Trim72, to ameliorate different features of the dystrophic phenotype and to bypass any metabolic alterations caused by the overexpression of Trim72. Importantly, the ectopic expression of either wild-type or nuclear HDAC4 in proliferating SCs did not rescue the mdx;KO, proving that HDAC4 is needed in the cytoplasm to exert its protective function in DMD. Actually, the forced expression of nuclear-restricted HDAC4 was even deleterious for mdx;KO muscle cell survival, probably due to its repressive activity on muscle structural genes.[1]

Fully in line with the above, we found that the protective role of HDAC4 in the mdx;KO cytoplasm does not entirely rely on HDAC4 deacetylase activity and may involve a novel HDAC4 function in regulating Trim72 mRNA stability, because increasing cytoplasmic HDAC4 in mdx;KO muscle correlates with higher Trim72 levels and improves muscle repair and regeneration. To the best of our knowledge, there are no data regarding the ability of HDAC4 to bind RNA in the literature. HDAC4 may affect Trim72 mRNA stability by associating with RNA binding proteins, as recently reported in the brain,[41] or via other HDAC members able to bind mRNAs.[42] This HDAC4 function resembles that of the HDAC SIRT1 in skeletal muscle, because defects in sarcolemma resealing were described in KO mice.[43] Further investigations are needed to verify a possible connection between HDAC4 and SIRT1, as already demonstrated in non-muscle cells, and to clarify the molecular mechanism that modulates mRNA or protein stability in DMD.

In conclusion, as summarized in *Figure* 8, our findings show that inhibiting HDAC4 is deleterious in DMD skeletal muscle. Additionally, we show that, unlike other HDACs, HDAC4 exerts relevant, so far neglected, cytoplasmic functions in dystrophic skeletal muscle. Therefore, we propose that forcing the extrusion of the endogenous HDAC4 from the nucleus, by means of phosphatase inhibitors, or the delivery of the cytoplasmic-restricted HDAC4 L/A protein to skeletal muscle may be considered as pharmacological or genetic approaches to ameliorate the condition of dystrophic muscles.

Acknowledgements

We are grateful to Carla Ramina and Carmine Nicoletti for technical assistance and Eric N. Olson and Rhonda Bassel-Duby for providing HDAC4 conditional mutant mice. We thank the Myobank-AFM of the Institute of Myology (Paris, France) for human DMD samples. We thank Anna L. Colin Mazzotti for the English editing of the manuscript. All authors of this manuscript comply with the guidelines of ethical authorship and publishing in the *Journal of Cachexia, Sarcopenia and Muscle*.[44]

Conflict of interest

The authors declare no competing interest.

Funding

This work was supported by Ricerca Finalizzata (GR-2010-2311055) from the Italian Ministry of Health, AFM Telethon (20603 and 22522), and Sapienza Research Project (2018-2019-2020). D.C. is also supported by Emergence SiRIC Curamus 2021.

Online supplementary material

Additional supporting information may be found online in the Supporting Information section at the end of the article.

Supplementary materials. Figures S1-S12

References

1. Haberland M, Montgomery RL, Olson EN. The many roles of histone deacetylases in development and physiology: implications for disease and therapy. *Nat Rev Genet* 2009;**10**:32–42.
2. Wang AH, Yang X-J. Histone deacetylase 4 possesses intrinsic nuclear import and export signals. *Mol Cell Biol*. American Society for Microbiology 2001;**21**:5992–6005.
3. Luo L, Martin SC, Parkington J, Cadena SM, Zhu J, Ibebunjo C, et al. HDAC4 controls muscle homeostasis through deacetylation of myosin heavy chain, PGC-1α, and Hsc70. *Cell Rep* Elsevier BV 2019;**29**:749–763.e12.
4. Williams AH, Valdez G, Moresi V, Qi X, McAnally J, Elliott JL, et al. MicroRNA-206 delays ALS progression and promotes regeneration of neuromuscular synapses in mice. *Science (80-)* 2009;**326**:1549–1554.
5. Moresi V, Williams AH, Meadows E, Flynn JM, Potthoff MJ, McAnally J, et al. Myogenin and class II HDACs control neurogenic muscle atrophy by inducing E3 ubiquitin ligases. *Cell* 2010;**143**:35–45.
6. Pigna E, Renzini A, Greco E, Simonazzi E, Fulle S, Mancinelli R, et al. HDAC4 preserves skeletal muscle structure following long-term denervation by mediating distinct cellular responses. *Skelet Muscle* BioMed Central 2018;**8**:6.
7. Pigna E, Simonazzi E, Sanna K, Bernadzki KM, Proszynski T, Heil C, et al. Histone deacetylase 4 protects from denervation and skeletal muscle atrophy in a murine model of amyotrophic lateral sclerosis. *EBioMedicine* Elsevier BV 2019;**40**:717–732.
8. Marroncelli N, Bianchi M, Bertin M, Consalvi S, Saccone V, De Bardi M, et al. HDAC4 regulates satellite cell proliferation and differentiation by targeting P21 and Sharp1 genes. *Sci Rep*. Nature Publishing Group 2018;**8**:3448.
9. Renzini A, Marroncelli N, Noviello C, Moresi V, Adamo S. HDAC4 regulates skeletal muscle regeneration via soluble factors. *Front Physiol* Frontiers Media SA 2018;**9**:1387.
10. Colussi C, Gurtner A, Rosati J, Illi B, Ragone G, Piaggio G, et al. Nitric oxide deficiency determines global chromatin changes in Duchenne muscular dystrophy. *FASEB J* Wiley 2009;**23**:2131–2141.
11. Duan D, Goemans N, Takeda S, Mercuri E, Aartsma-Rus A. Duchenne muscular dystrophy. *Nat Rev Dis Prim* 2021;**7**:13.
12. Morgan JE, Prola A, Mariot V, Pini V, Meng J, Hourde C, et al. Necroptosis mediates myofibre death in dystrophin-deficient mice. *Nat Commun*. Nature Publishing Group 2018;**9**:3655.
13. McElhanon KE, Bhattacharya S. Altered membrane integrity in the progression of muscle diseases. In *Life Sci*. Elsevier Inc.; 2018. p 166–172.
14. Weisleder N, Takizawa N, Lin P, Wang X, Cao C, Zhang Y, et al. Recombinant MG53 protein modulates therapeutic cell membrane repair in treatment of muscular dystrophy. *Sci Transl Med* 2012;**4**:139ra85.
15. Mozzetta C, Consalvi S, Saccone V, Tierney M, Diamantini A, Mitchell KJ, et al. Fibroadipogenic progenitors mediate the ability of HDAC inhibitors to promote regeneration in dystrophic muscles of young, but not old Mdx mice. *EMBO Mol Med* 2013;**5**:626–639.
16. Bettica P, Petrini S, D'Oria V, D'Amico A, Catteruccia M, Pane M, et al. Histological effects of givinostat in boys with Duchenne muscular dystrophy. *Neuromuscul Disord* 2016;**26**:643–649.
17. Bruserud O, Stapnes C, Ersvær E, Gjertsen B, Ryningen A. Histone deacetylase inhibitors in cancer treatment: a review of the clinical toxicity and the modulation of gene expression in cancer cells. *Curr Pharm Biotechnol* Bentham Science Publishers Ltd 2007;**8**:388–400.
18. Li S, Czubryt MP, McAnally J, Bassel-Duby R, Richardson JA, Wiebel FF, et al. Requirement for serum response factor for skeletal muscle growth and maturation revealed by tissue-specific gene deletion in mice. *Proc Natl Acad Sci U S A* National Academy of Sciences 2005;**102**:1082–1087.
19. Liu N, Williams AH, Maxeiner JM, Bezprozvannaya S, Shelton JM, Richardson JA, et al. MicroRNA-206 promotes skeletal muscle regeneration and delays progression of Duchenne muscular dystrophy in mice. *J Clin Invest* 2012;**122**:2054–2065.
20. Bostick B, Yue Y, Long C, Marschalk N, Fine DM, Chen J, et al. Cardiac expression of a mini-dystrophin that normalizes skeletal muscle force only partially restores heart function in aged Mdx mice. *Mol Ther* 2009;**17**:253–261.
21. De Paola E, Forcina L, Pelosi L, Pisu S, La Rosa P, Cesari E, et al. Sam68 splicing regulation contributes to motor unit establishment in the postnatal skeletal muscle. *Life Sci Alliance* Rockefeller University Press 2020;**3**.
22. Pratt SJP, Shah SB, Ward CW, Kerr JP, Stains JP, Lovering RM. Recovery of altered neuromuscular junction morphology and muscle function in mdx mice after injury. *Cell Mol Life Sci* Birkhauser Verlag AG 2014;**72**:153–164.
23. Renzini A, Benedetti A, Bouché M, Silvestroni L, Adamo S, Moresi V. Culture conditions influence satellite cell activation and survival of single myofibers. *Eur J Transl Myol* 2018;**28**:7567.
24. Dimauro I, Pearson T, Caporossi D, Jackson MJ. A simple protocol for the subcellular fractionation of skeletal muscle cells and tissue. *BMC Res Notes* 2012;**5**.
25. Lemon DD, Horn TR, Cavasin MA, Jeong MY, Haubold KW, Long CS, et al. Cardiac HDAC6 catalytic activity is induced in response to chronic hypertension. *J Mol Cell Cardiol* 2011;**51**:41–50.
26. Cai C, Masumiya H, Weisleder N, Pan Z, Nishi M, Komazaki S, et al. MG53 regulates membrane budding and exocytosis in muscle cells. *J Biol Chem* 2009;**284**:3314–3322.
27. He B, Tang RH, Weisleder N, Xiao B, Yuan Z, Cai C, et al. Enhancing muscle membrane repair by gene delivery of MG53 ameliorates muscular dystrophy and heart failure in δ-sarcoglycan-deficient hamsters. *Mol Ther* Nature Publishing Group 2012;**20**:727–735.
28. Vega RB, Matsuda K, Oh J, Barbosa AC, Yang X, Meadows E, et al. Histone deacetylase 4 controls chondrocyte hypertrophy during skeletogenesis. *Cell* 2004;**119**:555–566.
29. Miska EA, Karlsson C, Langley E, Nielsen SJ, Pines J, Kouzarides T. HDAC4 deacetylase associates with and represses the MEF2 transcription factor. *EMBO J* John Wiley & Sons, Ltd 1999;**18**:5099–5107.
30. Fortunato F, Rossi R, Falzarano MS, Ferlini A. Innovative therapeutic approaches for Duchenne muscular dystrophy. *J Clin Med* 2021;**10**:820.
31. Mozzetta C, Minetti G, Puri PL. Regenerative pharmacology in the treatment of genetic diseases: the paradigm of muscular dystrophy. *Int J Biochem Cell Biol* 2009;**41**:701–710.
32. Zeng LS, Yang XZ, Wen YF, Mai SJ, Wang MH, Zhang MY, et al. Overexpressed HDAC4 is associated with poor survival and promotes tumor progression in esophageal carcinoma. *Aging (Albany NY)* Impact Journals LLC 2016;**8**:1236–1248.
33. Cai C, Weisleder N, Ko J-K, Komazaki S, Sunada Y, Nishi M, et al. Membrane repair defects in muscular dystrophy are linked to altered interaction between MG53, caveolin-3, and dysferlin. *J Biol Chem* 2009;**284**:15894–15902.
34. Waddell LB, Lemckert FA, Zheng XF, Tran J, Evesson FJ, Hawkes JM, et al. Dysferlin, annexin A1, and mitsugumin 53 are upregulated in muscular dystrophy and localize to longitudinal tubules of the T-system with stretch. *J Neuropathol Exp Neurol* 2011;**70**:302–313.
35. Chang NC, Chevalier FP, Rudnicki MA. Satellite cells in muscular dystrophy—lost in polarity. *Trends Mol Med* Elsevier Ltd 2016;**22**:479–496.
36. De Luna N, Gallardo E, Soriano M, Dominguez-Perles R, De La Torre C, Rojas-García R, et al. Absence of dysferlin alters myogenin expression and delays human muscle differentiation "in vitro". *J Biol Chem* 2006;**281**:17092–17098.
37. Glover LE, Newton K, Krishnan G, Bronson R, Boyle A, Krivickas LS, et al. Dysferlin overexpression in skeletal muscle produces a progressive myopathy. *Ann Neurol* 2010;**67**:384–393.
38. Song R, Peng W, Zhang Y, Lv F, Wu HK, Guo J, et al. Central role of E3 ubiquitin ligase MG53 in insulin resistance and metabolic disorders. *Nature* 2013;**494**:375–379.
39. Liu F, Song R, Feng Y, Guo J, Chen Y, Zhang Y, et al. Upregulation of MG53 induces

diabetic cardiomyopathy through transcriptional activation of peroxisome proliferation-activated receptor α. *Circulation* Lippincott Williams and Wilkins 2015; **131**:795–804.
40. Yi J-S, Park JS, Ham Y-M, Nguyen N, Lee N-R, Hong J, et al. MG53-induced IRS-1 ubiquitination negatively regulates skeletal myogenesis and insulin signalling. *Nat Commun* 2013;**4**:2354.
41. Federspiel JD, Greco TM, Lum KK, Cristea IM. Hdac4 interactions in huntington's disease viewed through the prism of multiomics. *Mol Cell Proteomics*. American Society for Biochemistry and Molecular Biology Inc. 2019;**18**:S92–S113.
42. Albihlal WS, Gerber AP. Unconventional RNA-binding proteins: an uncharted zone in RNA biology. *FEBS Lett* Wiley Blackwell 2018;**592**:2917–2931.
43. Fujiwara D, Iwahara N, Sebori R, Hosoda R, Shimohama S, Kuno A, et al. SIRT1 deficiency interferes with membrane resealing after cell membrane injury. *PLoS ONE*. Public Library of Science 2018;**14**.
44. von Haehling S, Morley JE, Coats AJS, Anker SD. Ethical guidelines for publishing in the Journal of Cachexia, Sarcopenia and Muscle: update 2019. *J Cachexia Sarcopenia Muscle* 2019;**10**:1143–1145.

DOI: 10.1002/jcsm.12891